The Secondary Crest Myofibroblast PDGFRα Controls Elastogenesis Pathway via a Secondary Tier of Signaling Networks During Alveologenesis

Li C[1,*], Lee MK[1], Gao F[1], Webster S[1], Di H[1], Duan J[2], Yang C-Y[3], Bhopal N[1], Peinado N[1], Pryhubar G[4], Smith SM[1], Borok Z[5], Bellusci S[1,6], and Minoo P[1,*]

1. Department of Pediatrics, Division of Newborn Medicine, University of Southern California and Childrens Hospital Los Angeles, Los Angeles, CA 90033.

2. Department of Pediatrics, First Affiliated Hospital of Kunming Medical University, Kunming, Yunnan, China.

3. Department of Pediatrics, Chang Gung Children's Hospital and Chang Gung Memorial Hospital, Chang Gung University College of Medicine, Taoyuan, Taiwan.

4. Department of Pediatrics, University of Rochester Medical Center, Rochester, NY

5. Hastings Center for Pulmonary Research and Division of Pulmonary, Critical Care and Sleep Medicine, Department of Medicine, Keck School of Medicine, University of Southern California

6. Excellence Cluster Cardio-Pulmonary System (ECCPS), Universities of Giessen and Marburg Lung Center (UGMLC), Justus-Liebig-University Giessen, German Center for Lung Research (DZL), Giessen, Germany.

* authors for correspondence: changgon@usc.edu & minoo@usc.edu

ABSTRACT

Postnatal alveolar formation is the most important and the least understood phase of lung development. Alveolar pathologies are prominent in neonatal and adult lung diseases. The mechanisms of alveologenesis remain largely unknown. We inactivated *Pdgfra* postnatally in secondary crest myofibroblasts (SCMF) a subpopulation of lung mesenchymal cells. Lack of *Pdgfra* arrested alveologenesis akin to bronchopulmonary dysplasia, BPD, a neonatal chronic lung disease. Transcriptome of mutant SCMF revealed 1808 altered genes encoding transcription factors, signaling and extracellular matrix molecules. Elastin mRNA was reduced, and its distribution was abnormal. Absence of *Pdgfra* disrupted expression of elastogenic genes, including members of *Lox, Fbn,* and *Fbln* families. Expression of EGF family members increased while *Tgfb1* was repressed. Similar, but not identical results were found in human BPD lung samples. In vitro, blocking PDGF signaling decreased elastogenic gene expression associated with increased *Egf* and decreased *Tgfb* mRNAs. The effect was reversible by inhibiting EGF or activating TGFβ signaling. These observations demonstrate the previously unappreciated postnatal role of PDGFA/PDGFRα in controlling elastogenic gene expression via a secondary tier of signaling networks composed of EGF and TGFb.

INTRODUCTION

The mammalian lung is an efficient gas exchange organ. This capability is owed to the vast surface area, generated during postnatal development by a process known as alveolar formation or alveologenesis. At completion, alveologenesis in human lungs produces millions of alveoli, expanding the functional gas exchange surface area to nearly 100 square meters. Perturbations in development, or destruction of alveoli are causative or associative of a wide spectrum of both neonatal and adult human pulmonary diseases (Husain et al., 1998; Boucherat et al., 2016).

Alveologenesis in humans occurs mostly, and in mice entirely postnatally. In contrast to the many key regulators of early lung morphogenesis (i.e branching morphogenesis), the identity and the mechanisms of action of various molecules in postnatal lung development, and assembly of alveoli remain largely unknown. Alveologenesis requires the formation of structures known as "secondary crests". They are comprised of cells with distinct lineage histories, including a highly specialized mesodermal cell type known as the secondary crest myofibroblast (SCMF, *aka* alveolar myofibroblast). SCMFs are initially PDGFRα^{pos}, but late in embryonic development become αSMA^{pos} and are found localized to the tip of the alveolar septa in close proximity to deposits of elastin (ELN). Until recently, SCMFs remained inaccessible to isolation & analysis. We and others have shown that SCMFs are a subclass of lung mesodermal cells that are targeted by hedgehog signaling, and thus can be tagged and isolated by *Gli1-cre^{ERT2}*, a high-fidelity hedgehog reporter (Ahn and Joyner, 2004; Li et al., 2015; Kugler et al., 2018).

Platelet-derived growth factor, PDGFA is critical for normal vertebrate development (Soriano 1997). In lung morphogenesis, PDGFA, and its sole receptor, PDGFRα constitute an axis of cross-communication between endodermal and mesodermal cells (Bostrom et al., 1996). The ligand is expressed by endodermal cells (Bostrom et al., 1996) while PDGFRα, is ubiquitously expressed throughout the lung mesoderm (Orr-Urtreger & Lonai, 1992). Recently, single cell RNA sequencing showed PDGFRα^{pos} cells are comprised of cell lineages that make distinct contributions to lung maturation and response to injury (Endale et al., 2017; Li et al, 2018). Homozygous deletion of *Pdgfa* results in alveolar hypoplasia and lethality at birth (Bostrom et al.,1996; Lindhal et al., 1997). Germline lack of PDGFRα is even more profoundly lethal and *Pdgfra* null mice die before embryonic day E16 (Bostrom, 2002). Cell-targeted inactivation of *Pdgfra* in *Transgelin (SM22)*-expressing cells also leads to a phenotype of alveolar hypoplasia (McGowan and McCoy, 2014). In the latter studies, deletion of *Pdgfa* or *Pdgfra* caused extensive cell death, making it impossible to rule out the possibility that the alveolar phenotype is the consequence of cell death, rather than directly

related to lack of PDGFA/PDGFRα signaling. In addition, the genetic approaches, using germline deletion, or conditional inactivation of *Pdgfa* or *Pdgfra* were not specific to the alveolar phase of lung development. Thus, the specific function of *Pdgfra* in postnatal alveologenesis, particularly in SCMF, the key mesodermal cell type in this process has remained unclear.

In the present study, we utilized *Gli1-cre*^{ERT2} to generate conditional homozygous mice carrying deletion of *Pdgfra* exon 1-4, in SCMF during postnatal lung development. This approach enabled us to examine the role of *Pdgfra* specifically during the process of alveologenesis and in a cell targeted manner. The results illustrate a complex and interdependent, cross-regulatory network, composed of multiple signaling pathways that converge to regulate normal elastogenesis in SCMF during postnatal development. Furthermore, the findings provide evidence for the potential nature and the mechanism of ELN fiber defects observed in various human alveolar pathologies, such as BPD.

RESULTS

Postnatal Inactivation of *Pdgfra* in SCMF: To examine the role of PDGFA/PDGFRα in SCMF during postnatal alveologenesis, we generated *Pdgfra*$^{flox/flox}$*; Gli1-cre*^{ERT2}*;ROSA26*^{mTmg} mice (heretofore *Pdgfra*^{Gli}, Materials and Methods) and induced recombination by Tamoxifen (TAM) on PN2. Oral application of TAM worked reproducibly without loss of newborn mice, an important obstacle in such studies. Therefore, this regimen was adopted throughout the rest of this study.

Inactivation of *Pdgfra* on PN2 caused approximately 30% reduction in total lung *Pdgfra* mRNA (Figure 2). This is consistent with selective inactivation of *Pdgfra* by *Gli1-cre*^{ERT2} in SCMFs which as a subpopulation comprises approximately 20 percent of the total alveolar cell population (Figure 2). Histology of multiple biological replicates of *Pdgfra*^{Gli1} lungs at PN7 and PN14 showed profoundly arrested alveolar phenotype (Figure 1). Morphometric analysis revealed a 1.2 to 1.5 fold increase in mean linear intercept (MLI, $p<0.05$ for PN7 and PN14), coupled to 23% to 36% decrease in the number of secondary crests per unit area ($p<0.05$ for PN7 and PN14). Thus, postnatal *Pdgfra* inactivation selectively in SCMF is sufficient to produce an arrested phenotype nearly comparable to germline, global deletion of *Pdgfa* reported by previous studies indicating the importance of this cell type in alveologenesis (Bostrom et al, 1996; Lindahl et al., 1997).

Proliferation and Apoptosis in *Pdgfra*^{Gli1} Lungs: PDGFA/PDGFRα is a known regulator of cell proliferation (Kimani et al., 2009). We examined whether the observed *Pdgfra*^{Gli1} phenotype is caused by alterations in cell proliferation or apoptosis. Quantification of Ki67^{pos} cells using multiple samples of 3 independent biological replicates, showed a trend consistent with increased proliferation in the mutant lungs, although the difference did not reach statistical significance (p=0.07, Supplemental Figure 1). Similarly, while there was a seemingly decreased number of TUNEL^{pos} cells, the difference was not significant (p=0.13, Supplemental Figure 1). While these direct analyses indicate that conditional postnatal inactivation of *Pdgfra* does not result in significant cell death in *Pdgfra*^{Gli1} lungs, transcriptomic data showed cell survival as a major functional pathway associated with loss of *Pdgfra* (Figure 5). It is possible that this discrepancy may simply reflect the resolution of RNAseq technology compared with the other two more direct and specific analyses described in this section. To test this possibility, we defined the fate of targeted SCMF lacking PDGFRα activity, beginning on PN2 by comparing, in parallel, the relative ratio of GFP^{pos} cells to total alveolar cell counts in control and mutant lungs. This analysis revealed no change in the relative ratio of GFP^{pos} cells in the two lungs, indicating absence of selective loss of mutant SCMF (Figure 2). Thus, these observations indicate that the consequences of conditional inactivation of *Pdgfra* in the postnatal period contrast sharply with the previously reported significant loss of PDGFRα^{pos} cells resulting from global deletion of *Pdgfa* (Bostrom et al., 1996), suggesting potential differences between the embryonic versus postnatal function of PDGFA/PDGFRα signaling.

Cell Differentiation in *Pdgfra*^{Gli1} Lungs: Information on postnatal cross-communication amongst various cell types that make up the secondary crest structures during alveologenesis is lacking. To determine whether blocked PDGFA/PDGFRα signaling in SCMF disrupts cross-communication that may be required for maintenance or differentiation of other cell types, we used quantitative RT-PCR (qRT-PCR) to measure the expression of various cell type-specific markers. *SftpC*, a marker of alveolar epithelial type 2 cells (AT2) was statistically unchanged (relative mRNA ratio: 0.90) (Figure 3E). However, actual cell counts for AT2 cells, using multiple tissue preparations, immunostained with anti-SFTPC antibody revealed that the average number of SFTPC^{pos} cells as a fraction of total alveolar cells was significantly reduced in the mutant lungs (*15.8 +/-1.1% in control versus 12.2+/-0.8% in mutants, p<0.05*) (Figure 3F). The decrease in SFTPC^{pos} ratio was not associated with decrease in proliferating SFTPC^{pos} cells as determined by double immunostaining using Ki67 and SFTPC antibodies (Figure 3G). Quantitative RT-PCR showed no significant change in mRNA for multiple AT1 cell markers, including *Aqp5, Pdpn, Hopx* and *Rage* (Figure 3E). Consistent with the RNA results, ratio of HOPX^{pos} to total

alveolar cells was not significantly changed between the control and mutant lungs (Figure 3H). Thus, postnatal inactivation of *Pdgfra* in SCMF reduces the relative abundance or differentiation of AT2 cells. In mesodermal lineages, the only detectable impact was on *αSma* (0.49, $p<0.05$), while markers for pericytes (i.e. *Ng2, Pdgfrb*) and endothelial cells (*CD31, Flk1, Vegfa, Emcn*) remained unchanged (Figure 4). Consistent with these results there was no discernible difference between control and mutant lungs in Endomucin (EMCN) expression pattern (Figure 4).

Secondary Crest Formation Requires *Pdgfra* Activity: Secondary crests are identifiable as structures that physically arise from the primary septa and protrude into and divide the saccular space into smaller alveoli. In control lungs, we found immunoreactively positive cells for both GFP, marking SCMF, and PDGFRα localized to histologically identifiable secondary crest structures (Figure 2). In contrast, many of the GFP^{pos} cells in the $Pdgfra^{Gli1}$ lungs were $PDGFR\alpha^{neg}$ (Figure 2). These mutant GFP^{pos} cells were flat in shape compared to the controls that were round and localized to the tip of the normally formed secondary crests (Figure 2). The flat-shaped cells likely represent progenitors, or nascent SCMFs that remained within the primary septa, and failed to give rise to secondary crests, due to lack of PDGFRα activity. They account for the differences in the total number of secondary crests between the control and the mutant lungs as shown in Figure 1. Thus, formation of the secondary crests during postnatal alveologenesis requires the activity of PDGFRα.

Transcriptome of Isolated *$Pdgfra^{Gli1}$* SCMF: Cell-specific targets of the PDGFA/PDGFRa signaling network are not adequately known. In addition, these potential downstream targets particularly in neonatal lung have remained largely uncharacterized. Availability and access to GFP-labelled SCMF, lacking *Pdgfra,* and appropriate controls, presented the opportunity to define the gene expression profile of mutant SCMF, and investigate the potential downstream targets of PDGFA/PDGFRα signaling by comparative transcriptomic analysis. GFP^{pos} SCMF were isolated by FACS from control (*$mTmG^{Gli}$*) and $Pdgfra^{Gli1}$ lungs. The relative abundance of GFP^{pos} cells recovered by FACS from either control or mutant lungs was approximately 2% of the total sorted lung cells, again validating lack of significant cell death in $Pdgfra^{Gli1}$ lungs as shown in the previous sections (Supplemental Figure 1). Isolated GFP^{pos} cells were subjected to RNAseq and the data were analyzed by PartekFlow, Heatmapper and IPA.

Principal component analysis using two variables revealed significant differences in gene expression between the control and $Pdgfra^{Gli1}$ SCMF samples (Figure 5). There was a total of 1808 differentially expressed (DE) genes of which 866 increased, while 942 decreased in the

mutant SCMF (Figure 5). Functional enrichment analysis indicated that the mutant SCMF are altered in multiple biological processes. These include cellular movement, cell survival, and connective tissue development and functions (Figure 5). IPA analysis on potential upstream regulators showed alterations in multiple signaling pathways related to lung development. Interestingly, the top selected signaling pathways, included many purported regulators of the elastogenic process, including TGFβ, FGF2, IGF1 and EGF (reviewed by Sproul and Argraves, 2013) (Figure 5). A heatmap representation of the elastogenic gene cluster, shown in Figure 5, illustrates a clear trend towards decreased expression of this class of genes in the *Pdgfra*^{Gli1} SCMFs.

***Pdgfra* Regulates Genes in the Postnatal Elastogenesis Pathway:** Formation of secondary crests is dependent on expression and spatially correct distribution of elastin (ELN). Alterations in production &/or deposition of elastic fibers may be an important factor leading to arrested alveolar formation, such as that found in BPD (Bourbon et al., 2005). The RNA-seq analysis indicated alterations in a number of genes involved in production, assembly and deposition of ELN in *Pdgfra*^{Gli1} lungs. To validate the RNA-seq data, qRT-PCR was performed using RNA extracted from PN14 control and *Pdgfra*^{Gli1} lungs. The relative ratio of total *Eln* mRNA was lower by approximately 28% (p=0.09, Figure 6), even though no significant changes in *Eln* were detected by RNA-seq analysis. There was also reduced expression of Lysyl oxidases *Loxl1 (*0.53, p<0.05, Figure 6*)*. In addition, there was quantifiable reduction in the relative abundance of *Fbn2* (0.53, p=0.14), *Fbln1* (0.61, p<0.05) and *Fbln5* (0.50, p<0.05) in the mutant lungs. These data point to an encompassing dysregulation of multiple components of the elastogenic system in the *Pdgfra*^{Gli1} lungs, consistent with the SCMF RNA-seq data. Thus, while efficient *Eln* expression in the postnatal period is dependent on PDGFA/PDGFRα signaling, this pathway has far reaching impact on the complex elastogenic pathway.

To determine whether dysregulation of elastogenic genes resulted in alterations in processing or deposition of ELN fibers, we performed immunohistochemistry with anti-tropoelastin antibodies on PN14 lungs. In control lungs, tropoelastin was organized with a low to high gradient from primary septa to the tip of secondary crest, where it forms a concentrated moieties (Figure 6, arrows). In contrast to this pattern, ELN fibers in the *Pdgfra*^{Gli1} lungs were flat and spread along the walls of enlarged alveoli. This abnormal pattern of ELN deposition presumably is related to, or the cause of failure in septation and the consequent blocked alveolar phenotype in the mutant lungs (Figure 1).

Lack of *Pdgfra* in SCMF Alters Expression of Ligands in Secondary Signaling Pathways: To further examine the underlying causes of abnormal ELN distribution in *Pdgfra*^{Gli1} lungs, we examined the expression of signaling molecules uncovered by RNA-seq analysis in Figures 5D. A number of signaling networks are reported to be associated with elastogenesis (reviewed by Sproul and Argraves, 2013). Amongst these are TGFβ, IGF1, FGF2 and EGF. In *Pdgfra*^{Gli1} lungs, transcripts for *Tgfβ1* were not significantly changed (0.78, p=0.18) but there was a significant reduction in relative abundance of both *Tgfβ2* (0.54, p<0.05) & *Tgfβ3* (0.55, p<0.05). We also found a slight reduction in *Fgf2 (0.92, p<0.05),* while no significant change was detectable in *Igf1* and *Egf* family members (Figure 6).

To determine the direct impact of PDGFRα deficiency on SCMF, we prepared RNA from control and mutant FACS-isolated SCMFs (GFP^{pos}). qRT-PCR analysis showed significant reduction in *Pdgfra* (0.39, p<0.05), *Eln* (0.65, p<0.05), *Loxl1* (0.33, p<0.05), *Loxl4* (0.67, p<0.05). *Fbn2* (2.31, p=0.32), *Fbln1* (0.81, p=0.58), *Fbln2* (0.58, p=0.32) and *Fbln5* (1.52, p=0.52) also changed but did not reach statistical significance (Figure 7A). There was also quantifiable reduction in *Tgfb1* (0.68, p<0.05), while transcripts for several EGF family members [*Egf* (3.34, p=0.16), *Tgfα* (1.39, p=0.21) and *Btc* (3.17, p=0.13)] were increased in mutant SCMFs (Figure 7B).

The results of these *in vivo* findings suggest that PDGFA signaling regulates elastogenic gene expression. To test the validity of these findings, we isolated primary fibroblasts from PN5 lungs and cultured them in the presence or absence of two doses of imatinib, a well-established and widely used pharmacological inhibitor of the PDGFA/PDGFRα signaling pathway (McGowan and McCoy, 2011). As shown in Figure 7C, 10μM of imatinib reduced *Eln* (0.53, p<0.05), *Loxl1* (0.63, p<0.05), *Loxl4* (0.73, p<0.05), *Fbn2* (0.64, p<0.05) and *Fbln5* (0.66, p<0.05). Importantly, Imatinib decreased all three TGFβ transcripts [*Tgfb1* (0.60, p<0.05), *Tgfb2* (0.78, p=0.11), *Tgfb3* (0.66, p<0.05)], and increased mRNA for several EGF family members, including *Egf (3.41, p=0.11)*, *Tgfa (2.07, p<0.05)*, and *Btc (2.10, p<0.05)* (Figure 7D).

Blocking EGF Rescues ELN Abnormalities in Lung Fibroblasts: The observation that members of the EGF family of genes were increased in isolated *Pdgfra*^{Gli1} SCMF in association with ELN abnormalities prompted us to investigate whether the impact of *Pdgfra* inactivation is mediated via EGF signaling. To this end, we first examined whether recombinant EGF inhibited expression of the elastogenic genes which we found to be dysregulated in *Pdgfra*^{Gli1} lungs. In cultured PN5 primary lung fibroblasts 20 ng/ml of human recombinant EGF repressed the steady state level of *Eln*

(*0.42, p<0.05*), *Loxl4* (*0.78, P<0.05*), *Fbn2* (*0.59, p<0.05*), *Fbln5* (*0.5, p<0.05*), but had minor impact on *Loxl1* (*0.85, p<0.05*) (Figure 8A). We next examined whether treatment of PN5 cells with gefitinib a potent pharmacological inhibitor of EGFR could rescue the impact of imatinib-inhibition on the same elastogenic genes. In each case 1 μM of gefitinib almost completely reversed the inhibitory effect of imatinib and almost restored normal levels of *Loxl1*, *Loxl4*, *Fbn2,* and *Fbln5* (Figure 8). However, gefitinib failed to rescue imatinib-induced inhibition of *Eln*. Thus, with the exception of *Eln*, increased EGF mediates repression of this cluster of elastogenic genes induced by inhibition of PDGFA signaling. We next addressed the role of TGFβ signaling by examining whether recombinant TGFβ1 could rescue the imatinib-inhibited elastogenic gene cluster. As shown in Figure 8, TGFβ1 increased *Eln* expression, and more importantly, overcame the inhibitory effect of imatinib. TGFβ1 also partially rescued *Loxl1* but failed to rescue other elastogenic genes. Therefore, lack of signaling via PDGFRα alters EGF and TGFβ, which differentially regulate elastogenic genes in lung fibroblasts. In sum, EGF negatively regulates *Loxl1, Loxl4, Fbn2* and *Fbln5* while TGFβ1 positively regulates *Eln* and *Loxl1*. These findings illustrate the complex role of PDGFA/PDGFRα in a multi-signaling, interactive regulatory network that ultimately controls the expression of a battery of elastogenic genes necessary for normal alveolar formation in the postnatal period.

Dysregulated Elastogenic Gene Cluster in Human BPD: To examine the relevance of our mouse findings to human lung alveolar diseases, we analyzed expression of the elastogenic genes described above in de-identified human BPD samples. Histological assessment of BPD is consistent with a phenotype of arrested alveolar development (Husain et al., 1998). This feature has been phenocopied in neonatal mice by various injuries, including exposure to hyperoxia (Dasgupta et al., 2009). We used lung samples from a total of 9 individuals who died in the neonatal period. Four of the samples, including #30, #50, #52 and #56 were from neonates who died with "no or very mild Respiratory Distress Syndrome or RDS" (death due to non-pulmonary causes). We chose these samples as "control" because while "normal" early embryonic human samples are available from abortions, bioethical reasons make postnatal samples extremely rare. Realtime quantitative RT-PCR of the mouse elastogenic genes in human BPD samples showed the expected large variability amongst different human samples. Despite this variability, there was a general trend towards decreased expression of *LOXL1, LOXL4* and *FBN2* as shown by the boxplot (Figure 9). However, expression of *HB-EGF,* a member of the EGF family, was significantly increased in human BPD samples ($p<0.05$, Figure 9B). Of interest, the direction of change in sample #14, an early BPD sample was always consistent with the mouse data (Figure 9). On the whole, the

findings in what is admittedly a limited number of human BPD samples appears to generally recapitulate the findings in the *Pdgfra*^{Gli1} mouse model.

DISCUSSION

Alveolar formation in the mouse occurs exclusively in the postnatal period. Few studies have addressed the specific postnatal mechanisms underlying this vitally important process. The first clues that the PDGFA/PDGFRα axis may have a role in alveologenesis came from global (null) deletions of *Pdgfa or Pdgfra* (Bostrom et al, 1996; Lindahl et al., 1997). However, the null genetic approach in general precludes the possibility of ascertaining whether a phenotype is the consequence of interrupting postnatal processes, or embryonic ones that precede it. *Pdgfra* is expressed throughout the lung mesoderm from the onset of its morphogenesis. In addition, the previous null deletion studies were postnatally lethal and resulted in ubiquitous lack of PDGFA/PDGFRα pathway and depletion of PDGFRα^{pos} cells due to widespread cell death (Lindahl et al., 1997). Thus, the role, if any, of the PDGFA/PDGFRα pathway in alveolar formation had remained unknown. Recently, postnatal depletion of PDGFRα^{pos} cells was shown to cause alveolar hypoplasia (Li et al., 2018). While a clear demonstration that the PDGFRα^{pos} cell population is specifically required for alveolar formation, the study could not address the specific function of PDGFA/PDGFRα signaling, also due to cell death.

In the present study, we show that postnatal inactivation of *Pdgfra*, targeted to SCMF, a sub-lineage of lung PDGFRα^{pos} cells causes an arrested alveolar phenotype, comparable to that caused by null mutations of *Pdgfa* or *Pdgfra*. Importantly however, unlike the previous studies, the arrested alveologenesis in *Pdgfra*^{Gli1} lungs occurs without widespread loss of GFP^{pos} SCMFs (Figure 2H). Furthermore, early postnatal inactivation of *Pdgfra* in SCMF did not appear to block their differentiation as shown by positive staining for αSMA in GFP^{pos} cells (Figure 4B). Whether αSMA immuno-intensity represents *αSma* RNA changes observed by qRT-PCR remains unknown due to inherent non-quantifiable nature of immunostaining (Figure 4E). Nevertheless, the findings of the present study have enabled us to draw two important conclusions regarding the function of PDGFA/PDGFRα signaling in lung development that were previously unrecognized. First, abrogation of PDGFA signaling via conditional inactivation of *Pdgfra* in the postnatal period does not alter the relative abundance of GFP^{pos}-SCMFs. This contrasts with significant loss of SCMFs in *Pdgfa(-/-)* lungs (Bostrom, 1996). Second, due to absence of cell death, the results provide the first direct evidence that postnatal signaling via PDGFRα is required for alveologenesis.

Alveologenesis requires significant cell migration as the secondary crests emerge from the primary septa to form alveoli. PDGFA/PDGFRα signaling regulates migration of lung mesenchymal cells (McGowan and McCoy, 2018). The conditional targeted genetic approach used in this study found alterations in gene expression consistent with defects in SCMF migration in *Pdgfra*^{Gli1} lungs. A large number of SCMFs in *Pdgfra*^{Gli1} lungs were flat in shape and spread out on primary septa, indicating the strong possibility of failed secondary crest eruption. IPA analysis of RNA-seq data revealed migration as the top affected cellular function in mutant SCMF (Figure 5). Cell migration is regulated by multiple genes, an important class of which encode members of the extracellular matrix proteins or ECM. We found robust and widespread changes in various Collagen mRNAs. Of the 112 ECM genes examined, 106 were changed greater than 2 fold with *p* value <0.05. With the exception of Col6a4, which in many organs is associated with fibrosis, we found decreased ECM molecules in *Pdgfra*^{Gli1} lungs. Collagen type IV isoforms including *Col4a3*, *Col4a4*, and *Col4a6* were significantly decreased. Type IV collagens localize to the basement membrane of epithelial and interstitial endothelial cells where SCMFs are anchored. In previous reports, Postnatal inactivation of Type IV collagen caused defective ELN production and deposition, defects in alveologenesis and epithelial cell differentiation (Loscertales, M et al.,2016). In our study, we also found significant changes in multiple integrins (e.g. *Itga4*:0.54, FDR:6.99E-02; *Itga7*:0.39, FDR:4.80E-09; *Itga8*:0.35, FDR:3.27E-14; *Itgb8*:0.46, 5.76E-04) which mediate cell-ECM interactions and are critical for cell migration. Alterations in lung collagen levels and disorganization of ECM fibers have been reported in preterm infants with BPD (Thibeault, 2003).

A recognized feature of alveolar defects associated with lack of *Pdgfa* or *Pdgfra* in various reported models is reduced or absent ELN synthesis &/or abnormal deposition (Lindahl et al., 1997; McGowan and McCoy 2014). The mechanisms have remained unknown. There is now reliable evidence that ELN synthesis and deposition occur in a biphasic manner (Branchfield et al., 2016). Global *Pdgfa* deletion, while not affecting tropoelastin before birth, is reported to cause complete absence of tropoelastin associated with widespread loss of PDGFRα^{pos} cells (Bostrom et al., 1996). Thus, whether PDGFA is required for *Eln* expression during alveologenesis had remained unknown. In our hands, postnatal inactivation of *Pdgfra* did not cause widespread cell death but reduced *Eln* expression in isolated SCMF. Therefore, PDGFA signaling appears to be at least partly required for efficient expression of *Eln* in SCMF (Figure 7). In addition, deposition of ELN fibers was clearly abnormal (Figure 6). Elastogenesis is a complex and highly regulated process (Sproul and Argraves, 2013). Disrupted elastogenesis leads to abnormal alveologenesis (Wendel et al., 2000; McGowan and McCoy 2014; Li et al., 2017). In the lung, the mechanisms that functionally link

PDGFRα and elastogenic genes had remained unknown. Of the five lysyl oxidases required for integrity and elasticity of mature ELN, *Loxl1* was significantly reduced in *Pdgfra*^{Gli1} lungs (Figure 6). In addition, we found dysregulation of *Fbn2, Fbln1*, and *Fbln5* mRNA, which encode three ECM proteins implicated in ELN assembly and deposition (Figure 6). In the mouse hyperoxia model, which also causes alveolar arrest, tropoelastin was dysregulated, while *Loxl1, Fbn2, and Fbln5*, remained unchanged (Bland et al., 2008). Thus, while ELN abnormalities may be a hallmark of alveolar injury, the underlying mechanisms and whether it involves dysregulated elastogenic genes may depend on the mode of experimentally-induced injury. In support of this hypothesis, we found that even though *Eln*, *Loxl1* and *Loxl4* were consistently reduced under all PDGF-deficient conditions, there was differential impact on *Fbn2, Fbln1, Fbln2* and *Fbln5,* depending on the experimental conditions (Figures 6, 7 and 8).

PDGFRa Controls a Second Tier of Signaling Networks: Transcriptome of control and mutant SCMF revealed alterations in key signaling networks implicated in the elastogenic process. We show that two such networks, EGF and TGFβ regulate the expression of elastogenic genes. The EGF family members, *Egf, Tgfa,* and *Btc* were increased in both mutant SCMF (Figure 7B) and PN5 fibroblasts treated with imatinib (Figure 7D). A number of EGF ligands including EGF, HB-EGF, BTC and TGFα interact with the tyrosine kinase receptor EGFR to affect proliferation, differentiation and survival (Siddiqui et al., 2012). EGF/EGFR signaling is a critical regulator of lung morphogenesis (Miettinen et al., 1997; Plopper CG et al., 1992). Disrupted expression of EGFR and its ligands EGF, TGFα and BTC have been reported in BPD (Strandjord TP et al.,1995; Cuna et al., 2015). In mice, our findings are consistent with the report that overexpression of *Btc* disrupts alveologenesis (Schneider et al., 2005). In contrast to mice, we found decreased *BTC* in human BPD samples (Figure 9E). Decreased *BTC* has been reported in other human BPD studies (Cuna et al;2015) and likely reflects a failed compensatory response, particularly in late BPD samples. Intriguingly, and again in contrast to the mouse lung, transcripts for *HB-EGF*, an EGF family member in human BPD lungs were increased, while *EGF* remained unchanged. In support of a role for EGF, we show that recombinant EGF treatment of PN5 lung fibroblasts inhibits *Eln*, *Loxl1*, *Loxl4, Fbn2* and *Fbln5*. Furthermore, we show that gefitinib a potent EGFR inhibitor can rescue and almost completely reverse the imatinib-induced inhibition of the same elastogenic genes, except *Eln*. In conclusion, regardless of the specific ligand, over-activation of the EGF pathway appears to be a common molecular mechanism in both human BPD and *Pdgfra*^{Gli1} mouse lungs.

Several studies have shown that EGF signaling indeed negatively regulates elastogenesis (Ichiro et al., 1990; LeCras et al., 2004; DiCamillo et al., 2006, Bertram and Hass, 2009).

Further analyses revealed that activation of ERK mediates EGF inhibition of elastogenesis. Inhibition of ERK blocked EGF effects on elastogenesis (Liu et al., 2003; DiCamillo et al., 2002; DiCamillo et al., 2006), while activation of ERK inhibited elastogenesis (Lannoy et al., 2014). Consistent with these reports, we found that levels of p-ERK were indeed increased in the *Pdgfra*^{Gli1} lungs (Supplemental Figure 2) where elastogenic gene expression was decreased. Finally, as a first attempt, we examined whether blocking EGF signaling *in vivo* would reverse the alveolar hypoplasia phenotype in *Pdgfra*^{GLi1} lungs. *Pdgfra*^{GLi1} pups were treated by oral gavage with Gefitinib on PN4. As shown in Supplemental Figure 3, Gefitinib failed to rescue the hypoplastic phenotype of *Pdgfra*^{GLi1} lungs. This is likely due to pleiotropic role of EGF in many important processes including cell proliferation and migration, which are also critical for alveologenesis.

The other second tier pathway affected by lack of PDGFRα is TGFβ. In the lung, the role of TGFβ appears dose- and time-dependent. Application of supraphysiologic dose of TGFβ or TGFβ induced via hyperoxia, arrests alveolar formation (Vicencio et al., 2004). In contrast, one study has shown that antibody-blockade of TGFβ derails alveologenesis in lung explants (Pieretti et al., 2014). We found TGFβ signaling in SCMFs to be important in regulating elastic fiber formation. Interestingly, our results show that TGFβ and EGF each regulate a distinct group of elastogenic genes with partial overlap. TGFβ controls *Eln* and *Loxl1*, while EGF regulates *Loxl1, Loxl4, Fbn2, Fbln1* and *Fbln5*. This illustrates the requirement for integration of multiple convergent signaling pathways in the genetic architecture of the elastogenesis regulatory network, whose overall function is critical for normal alveolar formation in the postnatal period (Figure 10).

Finally, we were intrigued by the findings that alterations in SCMF affects the AT2 cell abundance, represented by the reduced ratio of SFTPC^{pos} cells in the *Pdgfra*^{Gli} lungs (Figure 3). In 3D organoid cultures, unfractionated PDGFRa^{pos} cells are known to exhibit unique properties in supporting and promoting adult AT2 cell proliferation and differentiation (Barkauskas et al., 2013). In the adult lung, PDGFRα^{pos} cells were reported to be spatially located in close juxtaposition to AT2 cells, suggesting they are components of the alveolar epithelial niche environment (Nabhan et al., 2018; Zepp et al., 2017). These observations support an active, functional cross-talk between PDGFRα^{pos} and AT2 cells in adult lung. PDGFRα is expressed by both lipofibroblast and myofibroblasts in both neonatal and adult lungs (Barkauskas et al., 2013; McGowan and McCoy, 2014; Endale et al., 2017). However, the *Gli1-cre*^{ERT2} driver line used in the present study to inactivate *Pdgfra* is not known to target lipofibroblasts (Li et al; 2015). Therefore, it is highly likely that the reduced number of AT2 cells in *Pdgfra*^{Gli1} lungs is causally linked to lack of *Pdgfra* in SCMF. Thus, the

mechanism must involve alterations in signaling molecules that are expressed by mutant SCMF that otherwise mediate the process of cross-talk with the epithelial cells. Recent studies have identified several signaling candidates that regulate AT2 cell abundance. For example, canonical WNT signaling mediates maintenance of $SFTPC^{pos}/Axin2^{pos}$ alveolar epithelial progenitor pool (Frank et al., 2016). RNAseq data generated in our study showed a mixed response of WNT ligands to *Pdgfra* deficiency (*Wnt4*: 0.61, FDA:9.72 E-2; *Wnt5a:*2.04, FDA:5.14 E-47; *Wnt6*:3.62, FDA:3.57 E-2). The net effect of the latter changes on WNT activity in AT2 cells is difficult to predict and remains to be determined more specifically in future studies. Other signaling pathways such as FGF10, HGF and Notch have also been shown to regulate epithelial cell proliferation during development and during injury repair (Panos et al., 1996; McQualter et al., 2010; Vaughan et al., 2015). Interestingly, levels of *Fgf10* (0.33, FDA:3.74 E-10), *Hgf* (0.30, FDA:4.56 E-01) and the NOTCH ligand *Jag1* (0.47, FDA:5.93 E-10) were all decreased in the PDGFRα deficient SCMF cells. More detailed and directed studies that are needed to identify the ligand/receptor complements and the mechanisms that mediate the SCMF-AT2 cross-talk are currently underway.

MATERIALS & METHODS

Mouse breeding and genotyping: All animals were maintained and housed in pathogen-free conditions according to a protocol approved by The University of Southern California Institutional Animal Care and Use Committee (IACUC) (Los Angeles, CA, USA). *Gli1-cre^{ERT2};Rosa26^{mTmG}* mice (*mTmG^{Gli}*) were generated by breeding *Gli1-cre^{ERT2}* (Ahn and Joyner, 2004) and *Rosa26^{mTmG}* mice [*Gt(ROSA)26Sor$^{tm4(ACTB-tdTomato,-EGFP)Luo}$/J*, The Jackson Laboratory]. *mTmG^{Gli}* mice were then bred with the *Pdgfra$^{flox/flox}$* mice (The Jackson Laboratory, Stock No:006492) to generate *Gli1-cre^{ERT2};Rosa26^{mTmG};Pdgfra$^{flox/flox}$ (Pdgfra^{Gli1})* mice on C57BL genetic background. Genotyping of the transgenic mice was performed by PCR with genomic DNA isolated from mouse tails. Forward (F) and reverse primers (R) for transgenic mouse genotyping are listed below. Both male and female mice were used in each of the experiments.

Gli1-cre^{ERT2}: (forward) 5'-TAA AGA TAT CTC ACG TAC TGA CGG TG-3' and (reverse) 5'-TCT CTG ACC AGA GTC ATC CTT AGC-3'. *Pdgfra$^{flox/flox}$*: (Forward) 5'- CCC TTG TGG TCA TGC CAA AC-3', and (wt-Reverse) 5'- GCT TTT GCC TCC ATT ACA CTG G-3' and (flox-Reverse) 5'- ACG AAG TTA TTA GGT CCC TCG AC-3'.

Human Neonatal Lung Samples: Human lung tissue samples were obtained postmortem by expedited autopsy of preterm infants having the diagnoses of mild RDS, evolving and established BPD, and term infants as controls (no lung disease). Collection and processing of the lung samples as from the deceased were approved by the University of Rochester Institutional Review Board. Selected clinical details have been previously published (Bhattacharya, et al., 2012).

Immunofluorescent staining: Immunofluorescent staining was performed as previously described (Li et al., 2009). Five micrometer (um) paraffin sections of the lung tissue were deparaffinized and rehydrated with ethanol gradient series to water. After antigen retrieval with citrate buffer (PH6.0) tissue sections were blocked with normal serum and then incubated with primary antibodies at 4°C overnight. Combination of fluorescein anti-mouse and Cy3 anti-rabbit or anti-goat IgG (Jackson ImmunoResearch Laboratories, ING) was applied to detect specific primary antibodies. After washing with PBS containing 0.1% Triton X-100, the sections were mounted with VECTASHELD mounting medium with DAPI (4′,6-diamidino-2-phenylindole) to counterstain neuclei. Primary antibodies used in this study were authenticated by the commercial source or validated in our own preliminary studies. The antibodies are listed in Supplemental Table ST2.

Tamoxifen administration: Tamoxifen (Sigma, 8mg/ml in peanut oil) was administered by oral gavage to neonates at postnatal day 2 (PN2, 400ug each pup) with a plastic feeding needle (Instech Laboratories, PA). Lungs of *Pdgfra*^{Gli1} and littermate controls were collected at PN7 to PN14 for morphological, immunohistochemical and molecular biologic analyses.

Neonatal lung fibroblast isolation and treatment: Wild type neonatal lungs at PN5 were dissected in HBSS (GIBCO24020-117). Lungs were inflated with dispase, tied at the trachea, and then digested by continuous shaking in Dispase at 37°C for 15 minutes. At the end of the incubation, lung lobes were isolated by dissection, cut into small pieces, transferred into Miltenyi tubes in 5 ml HBSS, and dissociated with gentle MACS dissociator (Miltenyi Biotec. Inc., San Diego). The dissociated cells were diluted in DMEM containing 10% FBS, filtered through a 40 μm cell strainer to remove tissue debris and then pelleted by centrifugation at 1200 rpm for 5 min. After washing with PBS, cells were resuspended in DMEM containing 10% FBS, plated in cell culture plates and incubated at 37°C with 5% CO2 for 1 hour. After removing floating cells, the attached fibroblasts were washed with PBS and cultured in fresh medium. When the fibroblasts grew to near confluency, they were trypsinized and seeded on 12 well plates at 100,000 cells/well. At 80% confluency, the cells were washed with PBS and then treated with growth factor or inhibitors as indicated in each

experiment in DMEM containing 1% FBS. After 48 hours, the cells were collected for RNA analyses. The cells were authenticated for absence of contaminations.

RNA-seq analyses: *mTmG^{Gli}* and *Pdgfra^{Gli1}* lungs, which received TAM at PN2, were dissected at PN14. GFP^{pos} cells were sorted by flow cytometry directly into RLT define buffer at the USC stem cell flow cytometry core facility using the FACS Aria II (BD Biosciences, CA) cell sorter. RNA was extracted using Qiagen RNeasy Micro kit and then submitted to the Millard and Muriel Jacobs Genetics and Genomics Laboratory at Caltech for sequencing which was run at 50 bp, single end, and 30 million reading depth. The unaligned raw reads from aforementioned sequencing were processed on the PartekFlow platform. In brief, reads alignment and gene annotation & quantification were based on mouse genome (mm10) and transcriptome (GENECODE genes-release 7). Tophat2 and Upper Quartile were algorithms used for mapping and normalization. Differential Gene Expression was performed with PartekFlow's Gene Specific Analysis (GSA). The exported Differential Gene Expression dataset was further processed for visualization, gene ontology and pathway analysis with software including XLSTAT (an add-on of Microsoft Excel), Panther Classification System, Heatmapper (Babicki et al., 2016) and Ingenuity Pathway Analysis (IPA, Qiagen).

Realtime Quantitative Polymerase Chain Reaction (qRT-PCR): Expression of selected genes was quantified by Realtime PCR using a LightCycler with LightCycler Fast Start DNA Master SYBR Green I Kit (Roche Applied Sciences, IN) as previously described (Li et al., 2005). Relative ratios of a target gene transcript in *Pdgfra^{Gli1}* and littermate control lungs were calculated with the ΔΔCt method. Primers for Realtime PCR were designed by using the program of Universal ProbeLibrary Assay Design Center from Roche Applied Sciences (IN). Sequences of the primers are listed in supplemental Table ST1.

Statistics analysis: At least 3 biological replicates for each experimental group and at least two or more biological replicates for the control lungs were used for each morphometric analysis, cell counting and qRT-PCR analyses. Multiple images as indicated in each figure legend were used to count MLI, # of secondary crest, and tissue/airspace ratios (10x magnification), GFP^{pos} cell ratio (40x magnification), SFTPC^{pos} cell ratio (40x magnification), Ki67^{pos}/SFTPC^{pos} cell ratio (40x magnification), HOPX^{pos} cell ratio (20x magnification), Ki67^{pos} cell ratio (20x magnification), and TUNEL^{pos} cell ratio (10x magnification). MLI and # of secondary crest were measured manually. Tissue/airspace ratios were measured with Image J (NIH). Quantitative data are presented as average values +/- standard error of the mean. *P* values were calculated by two tailed Student's T test.

Acknowledgements

We thank Hongyan Chen, Claudia Wang and Kim Ngo for their excellent technical support. We thank Dr. Alexandra Joyner (Sloan Kettering Institute, NY) for providing and Dr. Arturo Alvarez-Buylla (UCSF, CA) for making available the *Gli1-cre*^{ERT2} mice.

Competing interests

The authors declare no competing or financial interests.

Funding

This work was supported by the National Institutes of Health [HL122764, HL143059, HL144932 (CL & PM); HL135747 (ZB & PM)] and the Hastings Foundation. ZB is Ralph Edgington Chair in Medicine, PM is Hastings Professor of Pediatrics.

Data availability

The RNA-seq data have been deposited with Gene Expression Omnibus (GEO) under the accession number GSE126457.

REFERENCES

Ahn, S., Joyner, A.L., 2004. Dynamic changes in the response of cells to positive hedgehog signaling during mouse limb patterning. Cell 118, 505-516.

Babicki, S., Arndt, D., Marcu, A., Liang, Y., Grant, J.R., Maciejewski, A., Wishart, D.S., 2016. Heatmapper: web-enabled heat mapping for all. Nucleic Acids Res 44, W147-153.

Barkauskas, C.E., Cronce, M.J., Rackley, C.R., Bowie, E.J., Keene, D.R., Stripp, B.R., Randell, S.H., Noble, P.W., Hogan, B.L., 2013. Type 2 alveolar cells are stem cells in adult lung. J Clin Invest 123, 3025-3036.

Bertram C., Hass R., 2009. Cellular senescence of human mammary epithelial cells (HMEC) is associated with an altered MMP-7/HB-EGF signaling and increased formation of elastin-like structures. Mech Ageing Dev 130, 657-69.

Bhattacharya, S., Go, D., Krenitsky, D.L., Huyck, H.L., Solleti, S.K., Lunger, V.A., Metlay, L., Srisuma, S., Wert, S.E., Mariani, T.J., Pryhuber, G.S., 2012. Genome-wide transcriptional profiling reveals connective tissue mast cell accumulation in bronchopulmonary dysplasia. Am J Respir Crit Care Med 186, 349-358.

Bland, R.D., Ertsey, R., Mokres, L.M., Xu, L., Jacobson, B.E., Jiang, S., Alvira, C.M., Rabinovitch, M., Shinwell, E.S., Dixit, A., 2008. Mechanical ventilation uncouples synthesis and assembly of elastin and increases apoptosis in lungs of newborn mice. Prelude to defective alveolar septation during lung development? Am J Physiol Lung Cell Mol Physiol 294, L3-14.

Bostrom, H., Gritli-Linde, A., Betsholtz, C., 2002. PDGF-A/PDGF alpha-receptor signaling is required for lung growth and the formation of alveoli but not for early lung branching morphogenesis. Dev Dyn 223, 155-162.

Bostrom, H., Willetts, K., Pekny, M., Leveen, P., Lindahl, P., Hedstrand, H., Pekna, M., Hellstrom, M., Gebre-Medhin, S., Schalling, M., Nilsson, M., Kurland, S., Tornell, J., Heath, J.K., Betsholtz, C., 1996. PDGF-A signaling is a critical event in lung alveolar myofibroblast development and alveogenesis. Cell 85, 863-873.

Boucherat O, Morissette MC, Provencher S, Bonnet S, Maltais F., 2016. Bridging Lung Development with Chronic Obstructive Pulmonary Disease. Relevance of Developmental Pathways in Chronic Obstructive Pulmonary Disease Pathogenesis. Am J Respir Crit Care Med 193, 362-75

Branchfield, K., Li, R., Lungova, V., Verheyden, J.M., McCulley, D., Sun, X., 2016. A three-dimensional study of alveologenesis in mouse lung. Dev Biol 409, 429-441.

Bourbon J, Boucherat O, Chailley-Heu B, Delacourt C., 2005. Control mechanisms of lung alveolar development and their disorders in bronchopulmonary dysplasia. Pediatr Res57, 38R-46R.

Cuna, A., Halloran, B., Faye-Petersen, O., Kelly, D., Crossman, D.K., Cui, X., Pandit, K., Kaminski, N., Bhattacharya, S., Ahmad, A., Mariani, T.J., Ambalavanan, N., 2015. Alterations in gene expression and DNA methylation during murine and human lung alveolar septation. Am J Respir Cell Mol Biol 53, 60-73.

DiCamillo S.J., Carreras I., Panchenko M.V., Stone P.J., Nugent M.A., Foster J.A., Panchenko M.P., 2002. Elastase-released epidermal growth factor recruits epidermal growth factor receptor and extracellular signal-regulated kinases to down-regulate tropoelastin mRNA in lung fibroblasts. J Biol Chem 277(21), 18938-46.

DiCamillo S.J., Yang S., Panchenko M.V., Toselli P.A., Naggar E.F., Rich C.B., Stone P.J., Nugent M.A., Panchenko M.P., 2006. Neutrophil elastase-initiated EGFR/MEK/ERK signaling counteracts stabilizing effect of autocrine TGF-beta on tropoelastin mRNA in lung fibroblasts. Am J Physiol Lung Cell Mol Physiol 291(2), L232-43.

Dasgupta, C., Sakurai, R., Wang, Y., Guo, P., Ambalavanan, N., Torday, J.S., Rehan, V.K., 2009. Hyperoxia-induced neonatal rat lung injury involves activation of TGF-{beta} and Wnt signaling and is protected by rosiglitazone. Am J Physiol Lung Cell Mol Physiol 296, L1031-1041.

Endale, M., Ahlfeld, S., Bao, E., Chen, X., Green, J., Bess, Z., Weirauch, M., Xu, Y., Perl, A.K., 2017. Dataset on transcriptional profiles and the developmental characteristics of PDGFRα expressing lung fibroblasts. Data Brief 13, 415-431.

Frank, D.B., Peng, T., Zepp, J.A., Snitow, M., Vincent, T.L., Penkala, I.J., Cui, Z., Herriges, M.J., Morley, M.P., Zhou, S., Lu, M.M., Morrisey, E.E., 2016. Emergence of a Wave of Wnt Signaling that Regulates Lung Alveologenesis by Controlling Epithelial Self-Renewal and Differentiation. Cell Rep 17, 2312-2325.

Husain, A.N., Siddiqui, N.H., Stocker, J.T., 1998. Pathology of arrested acinar development in postsurfactant bronchopulmonary dysplasia. Hum Pathol 29, 710-717.

Ichiro T, Tajima S, Nishikawa T., 1990. Preferential inhibition of elastin synthesis by epidermal growth factor in chick aortic smooth muscle cells. Biochem Biophys Res Commun 168(2):850-6.

Kimani, P.W., Holmes, A.J., Grossmann, R.E., McGowan, S.E., 2009. PDGF-Ralpha gene expression predicts proliferation, but PDGF-A suppresses transdifferentiation of neonatal mouse lung myofibroblasts. Respir Res 10, 119.

Kugler, M.C., Loomis, C.A., Zhao, Z., Cushman, J.C., Liu, L., Munger, J.S., 2017. Sonic Hedgehog Signaling Regulates Myofibroblast Function during Alveolar Septum Formation in Murine Postnatal Lung. Am J Respir Cell Mol Biol 57, 280-293.

Lannoy M., Slove S., Louedec L., Choqueux C., Journé C., Michel J.B., Jacob M.P., 2014. Inhibition of ERK1/2 phosphorylation: a new strategy to stimulate elastogenesis in the aorta. Hypertension 64, 423-30.

Le Cras T.D., Hardie W.D., Deutsch G.H., Albertine K.H., Ikegami M., Whitsett J.A., Korfhagen T.R., 2004. Transient induction of TGF-alpha disrupts lung morphogenesis, causing pulmonary disease in adulthood. Am J Physiol Lung Cell Mol Physiol 287(4):L718-29.

Li, C., Hu, L., Xiao, J., Chen, H., Li, J.T., Bellusci, S., Delanghe, S., Minoo, P., 2005. Wnt5a regulates Shh and Fgf10 signaling during lung development. Dev Biol 287, 86-97.

Li, C., Li, A., Li, M., Xing, Y., Chen, H., Hu, L., Tiozzo, C., Anderson, S., Taketo, M.M., Minoo, P., 2009. Stabilized beta-catenin in lung epithelial cells changes cell fate and leads to tracheal and bronchial polyposis. Dev Biol 334, 97-108.

Li, C., Li, M., Li, S., Xing, Y., Yang, C.Y., Li, A., Borok, Z., De Langhe, S., Minoo, P., 2015. Progenitors of secondary crest myofibroblasts are developmentally committed in early lung mesoderm. Stem Cells 33, 999-1012.

Li, R., Bernau, K., Sandbo, N., Gu, J., Preissl, S., Sun, X., 2018. Pdgfra marks a cellular lineage with distinct contributions to myofibroblasts in lung maturation and injury response. Elife 7, e36865.

Li, R., Herriges, J.C., Chen, L., Mecham, R.P., Sun, X., 2017. FGF receptors control alveolar elastogenesis. Development 144, 4563-4572.

Lindahl, P., Karlsson, L., Hellstrom, M., Gebre-Medhin, S., Willetts, K., Heath, J.K., Betsholtz, C., 1997. Alveogenesis failure in PDGF-A-deficient mice is coupled to lack of distal spreading of alveolar smooth muscle cell progenitors during lung development. Development 124, 3943-3953.

Liu J., Rich C.B., Buczek-Thomas J.A., Nugent M.A., Panchenko M.P., Foster J.A., 2003. Heparin-binding EGF-like growth factor regulates elastin and FGF-2 expression in pulmonary fibroblasts. Am J Physiol Lung Cell Mol Physiol 285, L1106-15.

Loscertales, M., Nicolaou, F., Jeanne, M., Longoni, M., Gould, D.B., Sun, Y., Maalouf, F.I., Nagy, N., Donahoe, P.K., 2016. Type IV collagen drives alveolar epithelial-endothelial association and the morphogenetic movements of septation. BMC Biol 14, 59.

McGowan, S.E., McCoy, D.M., 2011. Fibroblasts expressing PDGF-receptor-alpha diminish during alveolar septal thinning in mice. Pediatr Res 70, 44-49.

McGowan, S.E., McCoy, D.M., 2014. Regulation of fibroblast lipid storage and myofibroblast phenotypes during alveolar septation in mice. Am J Physiol Lung Cell Mol Physiol 307, L618-631.

McGowan, S.E., McCoy, D.M., 2018. Neuropilin-1 and platelet-derived growth factor receptors cooperatively regulate intermediate filaments and mesenchymal cell migration during alveolar septation. Am J Physiol Lung Cell Mol Physiol 315, L102-L115.

McQualter, J.L., Yuen, K., Williams, B., Bertoncello, I., 2010. Evidence of an epithelial stem/progenitor cell hierarchy in the adult mouse lung. Proc Natl Acad Sci 107, 1414-1419.

Miettinen, P.J., Warburton, D., Bu, D., Zhao, J.S., Berger, J.E., Minoo, P., Koivisto, T., Allen, L., Dobbs, L., Werb, Z., Derynck, R., 1997. Impaired lung branching morphogenesis in the absence of functional EGF receptor. Dev Biol 186, 224-236.

Nabhan, A.N., Brownfield, D.G., Harbury, P.B., Krasnow, M.A., Desai, T.J., 2018. Single-cell Wnt signaling niches maintain stemness of alveolar type 2 cells. Science 359, 1118-1123.

Orr-Urtreger, A., Lonai, P., 1992. Platelet-derived growth factor-A and its receptor are expressed in separate, but adjacent cell layers of the mouse embryo. Development 115, 1045-1058.

Panos, R.J., Patel, R., Bak, P.M., 1996. Intratracheal administration of hepatocyte growth factor/scatter factor stimulates rat alveolar type II cell proliferation in vivo. Am J Respir Cell Mol Biol 15, 574-581.

Pieretti, A.C., Ahmed, A.M., Roberts, J.D., Jr., Kelleher, C.M., 2014. A novel in vitro model to study alveologenesis. Am J Respir Cell Mol Biol 50, 459-469.

Plopper, C.G., St George, J.A., Read, L.C., Nishio, S.J., Weir, A.J., Edwards, L., Tarantal, A.F., Pinkerton, K.E., Merritt, T.A., Whitsett, J.A., et al., 1992. Acceleration of alveolar type II cell differentiation in fetal rhesus monkey lung by administration of EGF. Am J Physiol 262, L313-321.

Schneider, M.R., Dahlhoff, M., Herbach, N., Renner-Mueller, I., Dalke, C., Puk, O., Graw, J., Wanke, R., Wolf, E., 2005. Betacellulin overexpression in transgenic mice causes disproportionate growth, pulmonary hemorrhage syndrome, and complex eye pathology. Endocrinology 146, 5237-5246.

Siddiqui, S., Fang, M., Ni, B., Lu, D., Martin, B., Maudsley, S., 2012. Central role of the EGF receptor in neurometabolic aging. Int J Endocrinol 2012, 739428.

Soriano, P., 1997. The PDGF alpha receptor is required for neural crest cell development and for normal patterning of the somites. Development 124, 2691-2700.

Sproul, E.P., Argraves, W.S., 2013. A cytokine axis regulates elastin formation and degradation. Matrix Biol 32, 86-94.

Strandjord, T.P., Clark, J.G., Guralnick, D.E., Madtes, D.K., 1995. Immunolocalization of transforming growth factor-alpha, epidermal growth factor (EGF), and EGF-receptor in normal and injured developing human lung. Pediatr Res 38, 851-856.

Thibeault, D.W., Mabry, S.M., Ekekezie, I.I., Zhang, X., Truog, W.E., 2003.Collagen scaffolding during development and its deformation with chronic lung disease. Pediatrics 111, 766-76.

Vaughan, A.E., Brumwell, A.N., Xi, Y., Gotts, J.E., Brownfield, D.G., Treutlein, B., Tan, K., Tan, V., Liu, F.C., Looney, M.R., Matthay, M.A., Rock, J.R., Chapman, H.A., 2015. Lineage-negative progenitors mobilize to regenerate lung epithelium after major injury. Nature 517, 621-625.

Vicencio, A.G., Lee, C.G., Cho, S.J., Eickelberg, O., Chuu, Y., Haddad, G.G., Elias, J.A., 2004. Conditional overexpression of bioactive transforming growth factor-beta1 in neonatal mouse lung: a new model for bronchopulmonary dysplasia? Am J Respir Cell Mol Biol 31, 650-656.

Wendel, D.P., Taylor, D.G., Albertine, K.H., Keating, M.T., Li, D.Y., 2000. Impaired distal airway development in mice lacking elastin. Am J Respir Cell Mol Biol 23, 320-6.

Zepp, J.A., Zacharias, W.J., Frank, D.B., Cavanaugh, C.A., Zhou, S., Morley, M.P., Morrisey, E.E., 2017. Distinct Mesenchymal Lineages and Niches Promote Epithelial Self-Renewal and Myofibrogenesis in the Lung. Cell 170, 1134-1148 e1110.

Figures

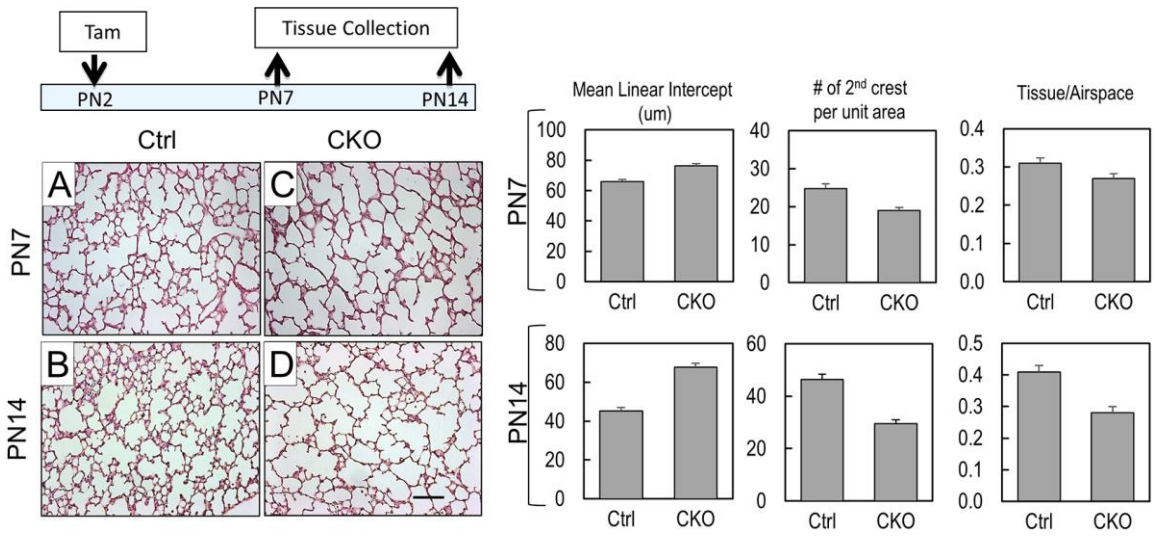

Figure 1. *Pdgfra* deficiency disrupts alveologenesis in *Pdgfra*^{Gli1} lungs. (**A-D**) Hematoxylin and eosin (H&E) staining of control (Ctrl, A&B) and *Pdgfra*^{Gli1} conditional knockout (CKO, C&D) lungs. Neonatal mice were treated with tamoxifen on postnatal day 2 (PN2) and lungs were analyzed on PN7 (A&C) and PN14(B&D). Scale bar: 100 μm. Multiple H&E images from 3 Ctrl and 3 CKO lungs were analyzed for mean linear intercept (MLI), number of secondary crests per unit area, and tissue/airspace ratio (PN7: Ctrl, n=15; CKO, n=20; PN14: Ctrl, n=13; CKO, n=13).

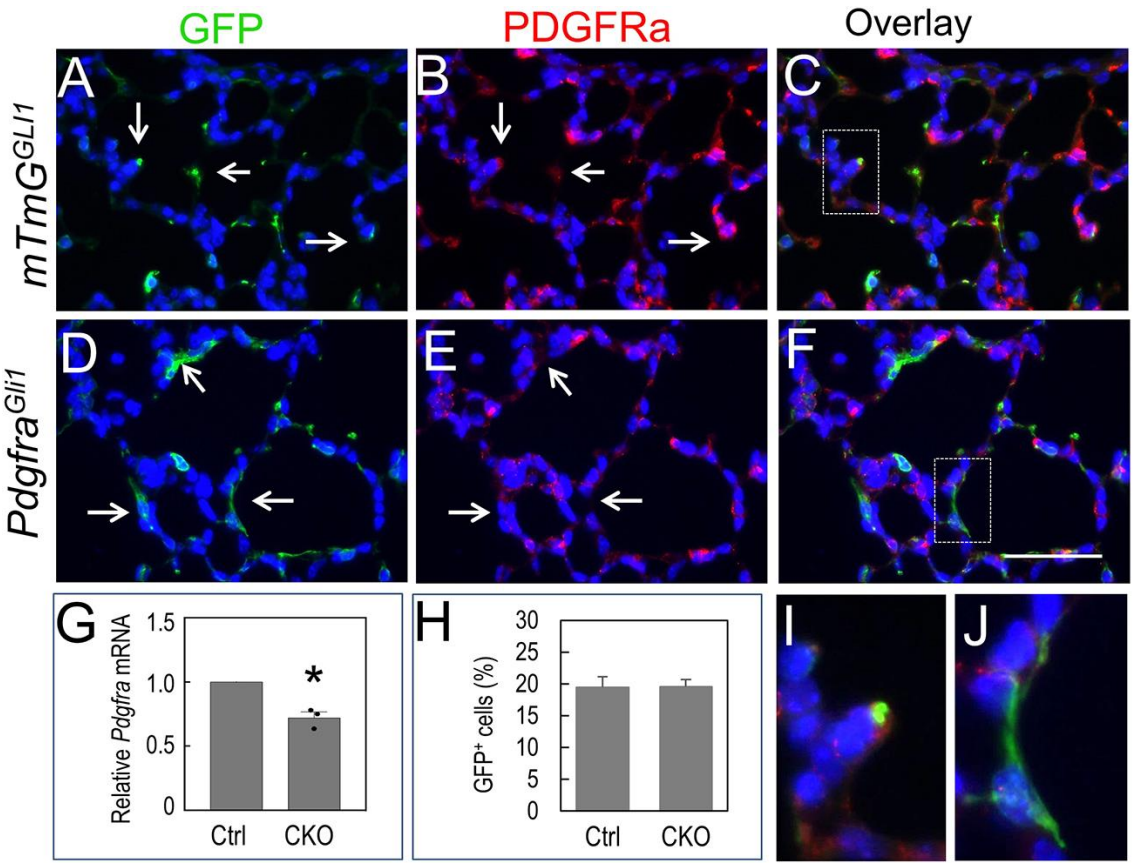

Figure 2. PDGFRα is targeted in SCMF of PN14 *Pdgfra*^{Gli1} lungs. (A-F) Double immunostaining of GFP and PDGFRα in PN14 control (*mTmG*^{Gli}, A-C) and *Pdgfra*^{Gli1} lungs (D-F). Arrows in panels A-C indicate PDGFRα positive staining in GFP^{pos} SCMF cells of control lungs. Arrows in panels D-E indicate PDGFRα negative staining in GFP^{pos} SCMF cells of *Pdgfra*^{Gli1} lungs. **(I&J)** show higher magnification of boxed areas in panel C & F, respectively. Scale bar: 50 μm for A-F, 11.6 μm for I & J. **(G)** shows that relative *Pdgfra* mRNA levels are reduced in *Pdgfra*^{Gli1} lungs (n=3). * indicates $p<0.05$. **(H)** shows that ratios of GFP^{pos} cells to DAPI^{pos} alveolar cells are similar between the control and mutant lungs. Multiple images from 3 ctrl and 3 CKO lungs were analyzed (Ctrl: n=11; CKO: n=11).

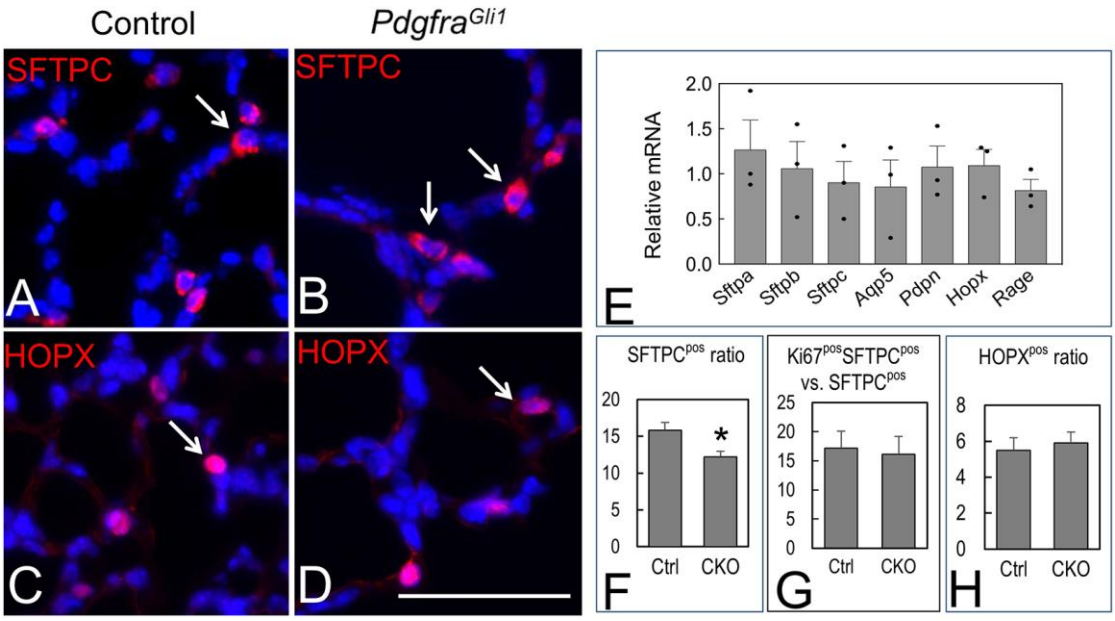

Figure 3. Epithelial cell differentiation in PN14 *Pdgfra*^{Gli1} lungs. (A-D) Immunostaining of SFTPC (A&B) and HOPX (C&D) in PN14 control (A&C) and *Pdgfra*^{Gli1} lungs (B&D). Nuclei were stained with DAPI. Scale bar: 32 μm. **(E)** qRT-PCR showing relative ratios of AT1 and AT2 markers in PN14 *Pdgfra*^{Gli1} to control lungs (n=3). **(F)** Ratios of SFTPC^{pos} to DAPI^{pos} alveolar cells. **(G)** Ratios of Ki67^{pos}/SFTPC^{pos} to SFTPC^{pos} cells. **(H)** Ratios of HOPX^{pos} to DAPI^{pos} alveolar cells. Data derived from multiple images from 3 ctrl and 3 CKO PN14 lungs (**F:** Ctrl, n=19; CKO, n=27; **G:** Ctrl, n=18; CKO, n=18; **H:** Ctrl, n=14; CKO, n=18). * indicates $p<0.05$. Each bar represents average +/- standard error of the mean (sem).

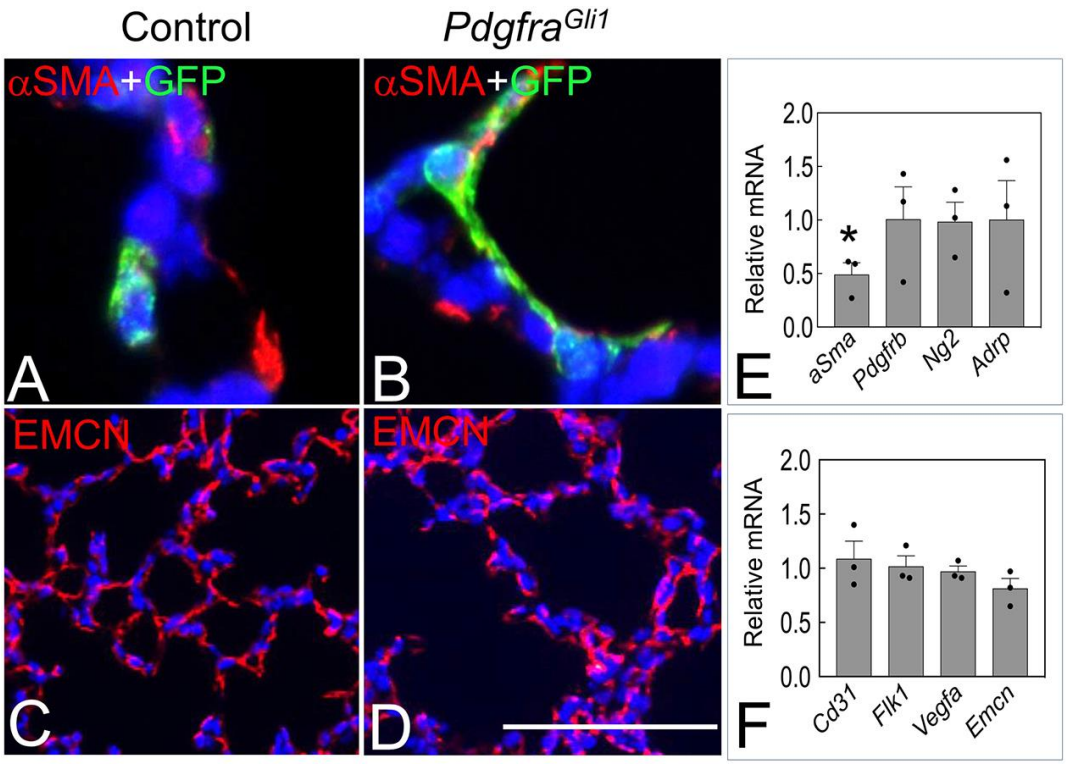

Figure 4. Mesenchymal cell differentiation in *Pdgfra*^{Gli1} lungs. (A&B) Double immunostaining of GFP and αSMA in PN14 control (A) and *Pdgfra*^{Gli1} lungs (B). **(C&D)** Immunostaining of EMCN in PN14 control (C) and *Pdgfra*^{Gli1} lungs (D). **(E&F)** qRT-PCR of relative mRNA levels of fibroblast markers (E) and endothelial markers (F) in PN14 *Pdgfra*^{Gli1} to control lungs (n=3). Each bar represents average +/-sem. * indicates $p<0.05$. Scale bar: 22 μm for A-B, 100 μm for C-D.

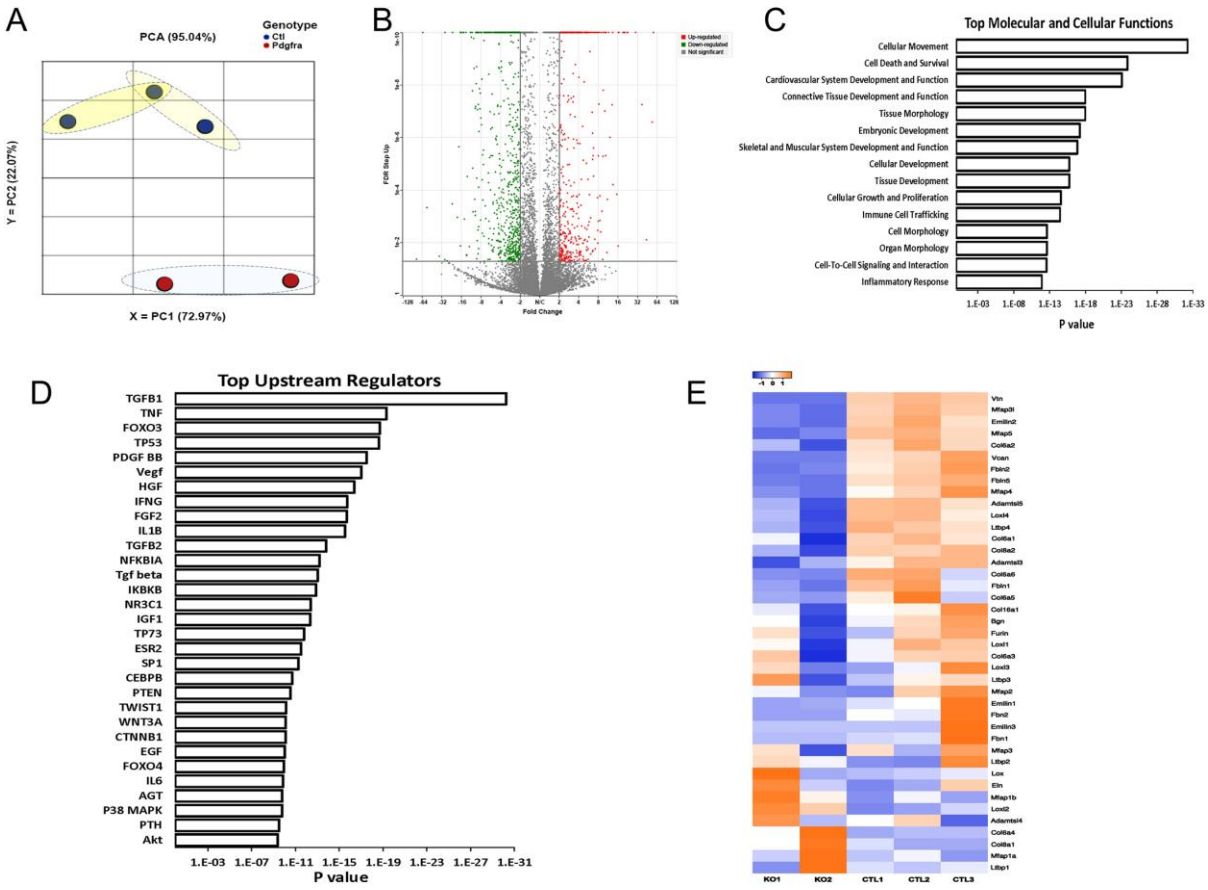

Figure 5. Transcriptome of GFP^{pos} SCMF. GFP^{pos} SCMF were isolated from PN14 control (*mTmG*^{Gli}) and *Pdgfra*^{Gli1} lungs by FACS and used for RNA-seq analyses. **(A)** Principle component analyses of 3 control and 2 mutant samples. (**B)** Volcano plot that shows the up-regulated (red) and down-regulated (green) genes ($p<0.05$, Fold changes>=2) in the mutant samples as compared to that of controls. **(C)** Top disrupted molecular and cellular functions identified by IPA analyses. **(D)** Top upstream regulators identified by IPA analyses. **(E)** Heatmap of elastogenic genes.

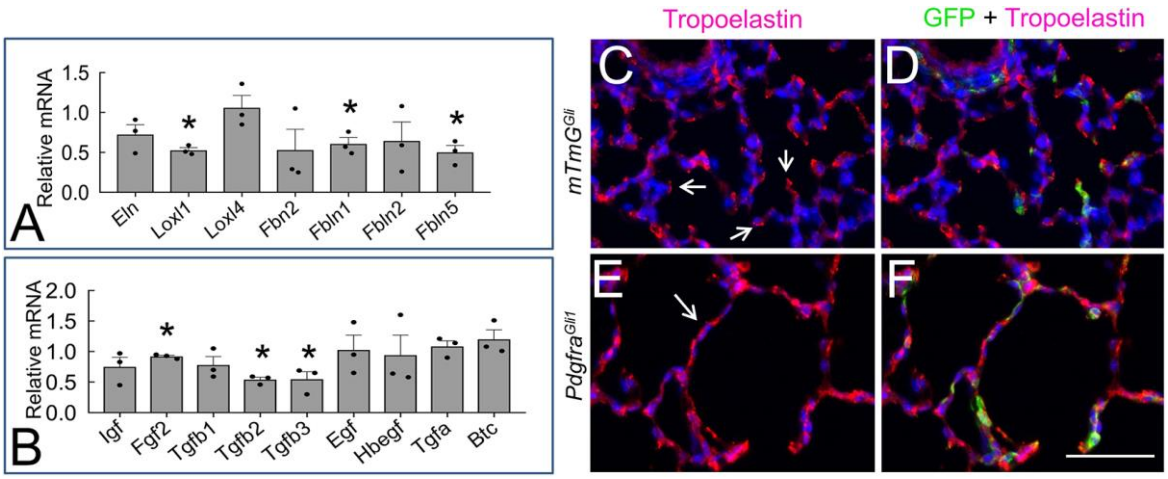

Figure 6. Elastin distribution is disrupted in PN14 *Pdgfra*^{Gli1} lungs. (A&B) qRT-PCR analyses of elastogenic genes (A) and signaling molecules that regulate elastogenesis (B) in PN14 control and mutant lungs (n=3). Each bar represents average ratio (mutant vs. control) +/-sem. * indicates $p<0.05$. **(C-F)** Double immunostaining of GFP and tropoelastin in PN14 control (C&D) and *Pdgfra*^{Gli1} lungs (E&F). Arrows in panel C indicate ELN deposition at the tips of secondary crests. Scale bar: 50 μm.

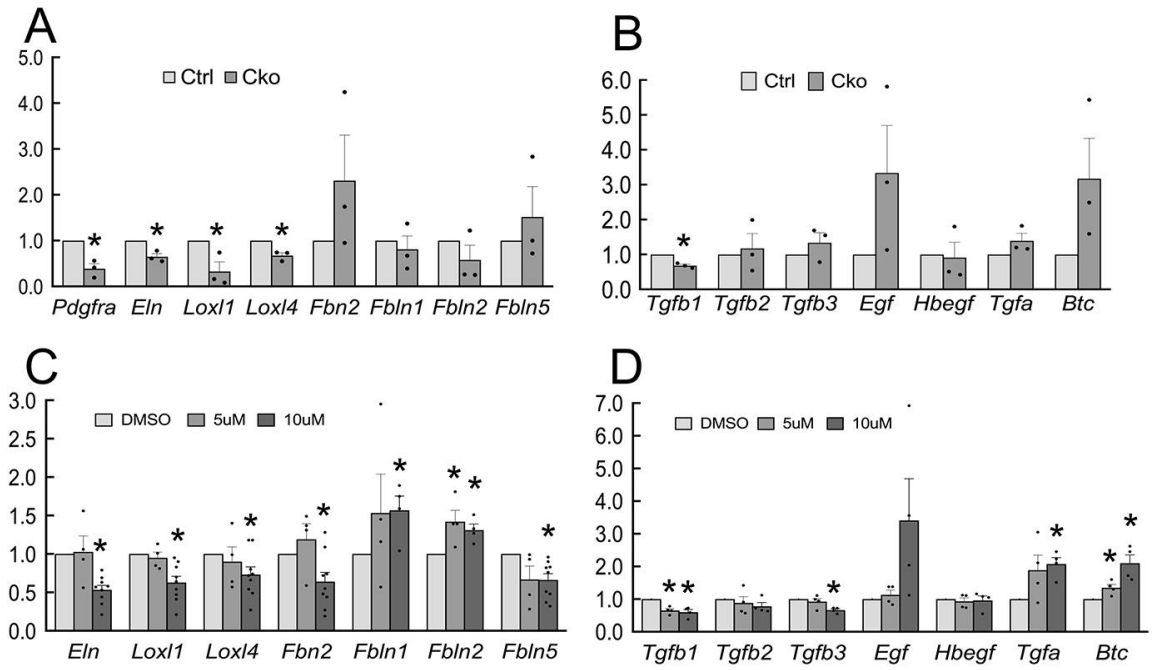

Figure 7. *Pdgfra* deficiency disrupts elastogenic gene expression. (A&B) qRT-PCR analyses of elastogenic genes and related signaling molecules in sorted GFP^{+} cells of PN14 control and *Pdgfra*^{Gli1} lungs (n=3). **(C&D)** qRT-PCR analyses of elastogenic gene and related signaling molecules in primary lung fibroblasts cultured in the presence of DMSO (Dimethyl sulfoxide, carrier, as control), 5uM or 10uM of Imatinib (n=4-9). * indicates $p<0.05$. Each bar represents average +/-sem.

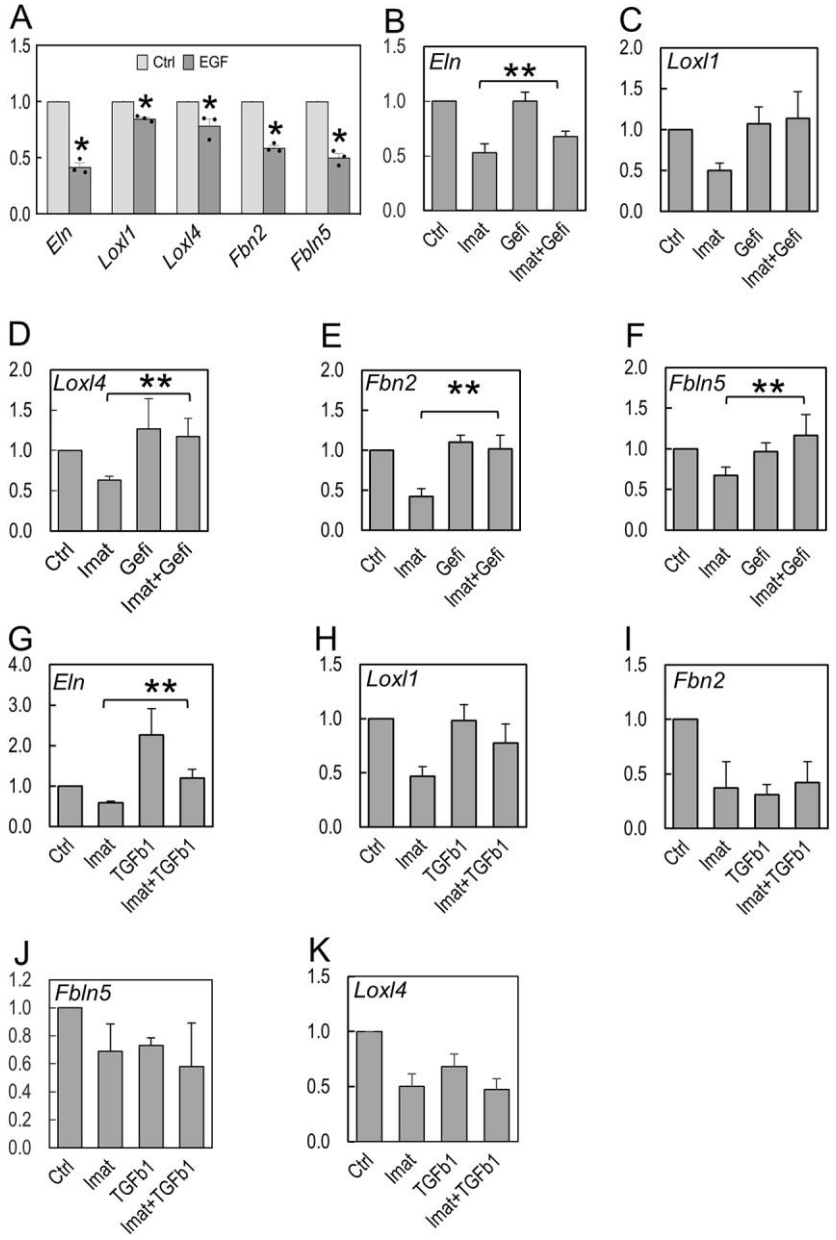

Figure 8. EGF and TGFβ differentially regulate elastogenic gene expression. (A) qRT-PCR analyses of elastogenic gene expression in primary lung fibroblasts cultured in presence of carrier or 20ng/ml of human EGF (n=3). * indicates $p<0.05$. **(B-F)** qRT-PCR analyses of elastogenic gene expression in primary lung fibroblasts cultured in presence of carrier (ctrl), 10um of imatinib (10 μM), gefitinib (1 μM), or imatinib plus gefitinib (n=5). **(G-K)** qRT-PCR analyses of elastogenic gene expression in primary lung fibroblasts cultured in the presence of carrier (ctrl), imatinib (10 μM), TGFβ1 (2 ng/ml), or imatinib plus TGFβ1 (n=5). * indicates $p<0.05$ when compared to Imat only condition (2nd bar in each group). Each bar represents average +/-sem.

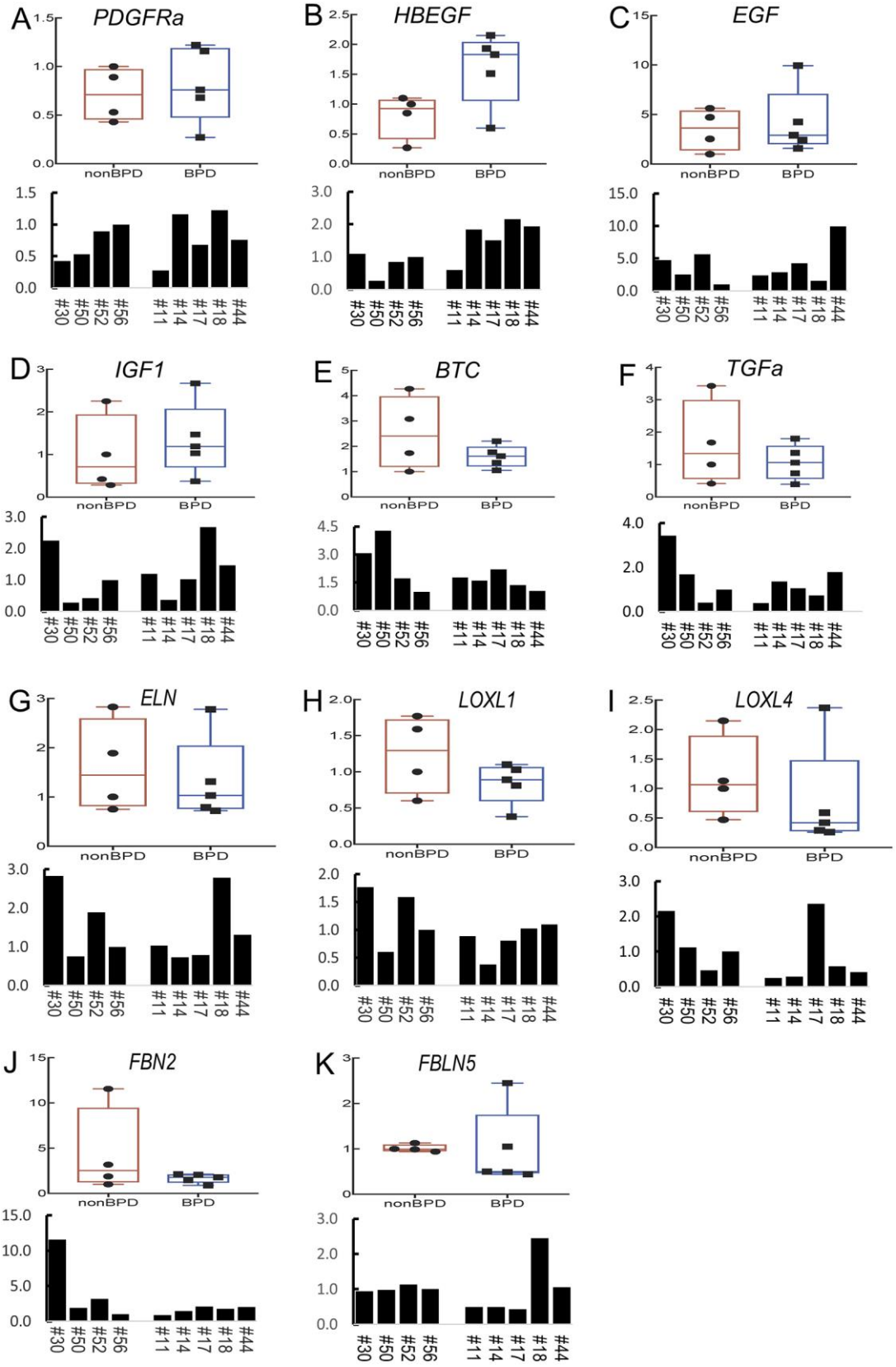

Figure 9. Elastogenic gene expression in human BPD lungs. qRT-PCR analyses of elastogenic genes and related signaling molecules in human BPD lung samples. Collection and processing of the lung samples from the deceased were conducted at University of Rochester and were approved by the University of Rochester Institutional Review Board. Samples #11, #14, #17, #18, and #44 were from BPD patients. Samples #30, #50, #52, #56 were from patients not diagnosed with BPD. The 2-D column chart shows relative mRNA levels of the tested gene (indicated in the chart) as compared to that of #56 (arbitrarily set as 1). The boxplot shows data distribution of non-BPD (left) and BPD (right) samples.

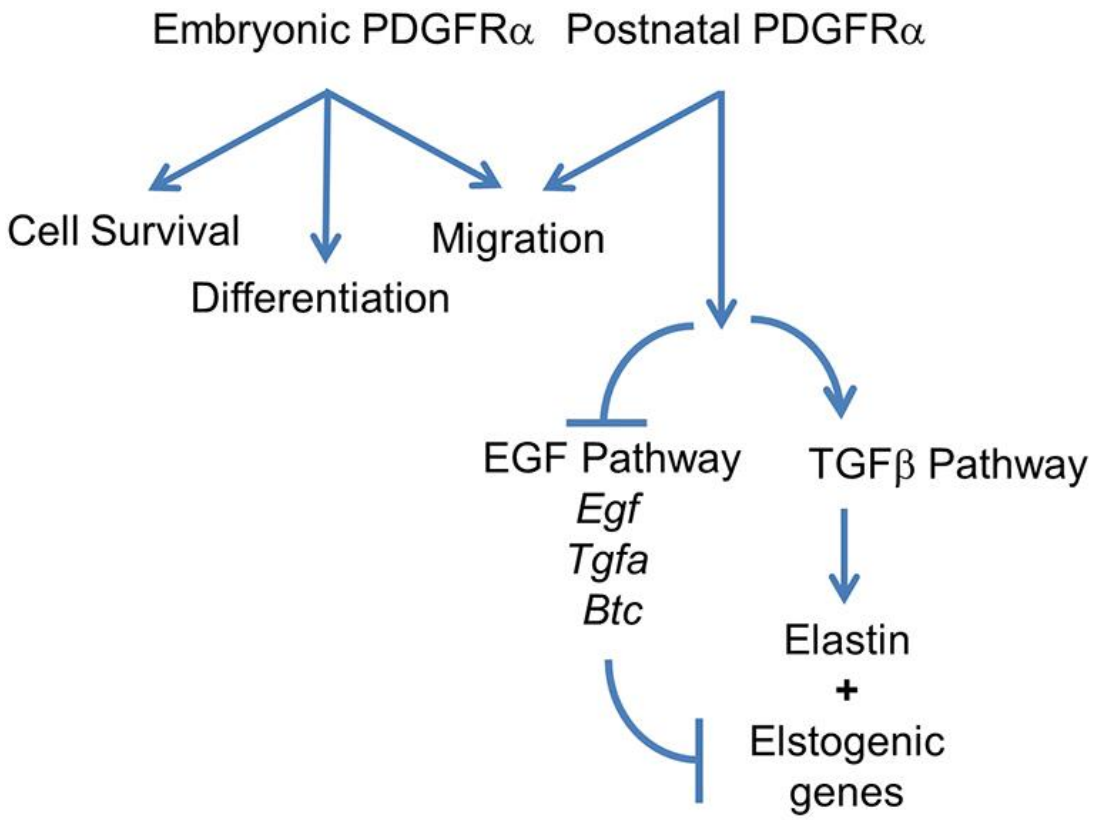

Figure 10. Simplified model illustrating PDGFRα functions in elastrogenesis. Previous studies showed that PDGFA is essential for migration and survival of PDGFRα^{pos} cells during embryonic development (Bostrom et al, 1996; Lindahl et al., 1997). Current study revealed the cell type specific function of PDGFRα during alveologenesis. Postnatal PDGFRα is critical in regulating elastogenesis, which involves EGF and TGFβ signaling. Arrows indicate positive regulation. Vertical lines indicate negative regulation.

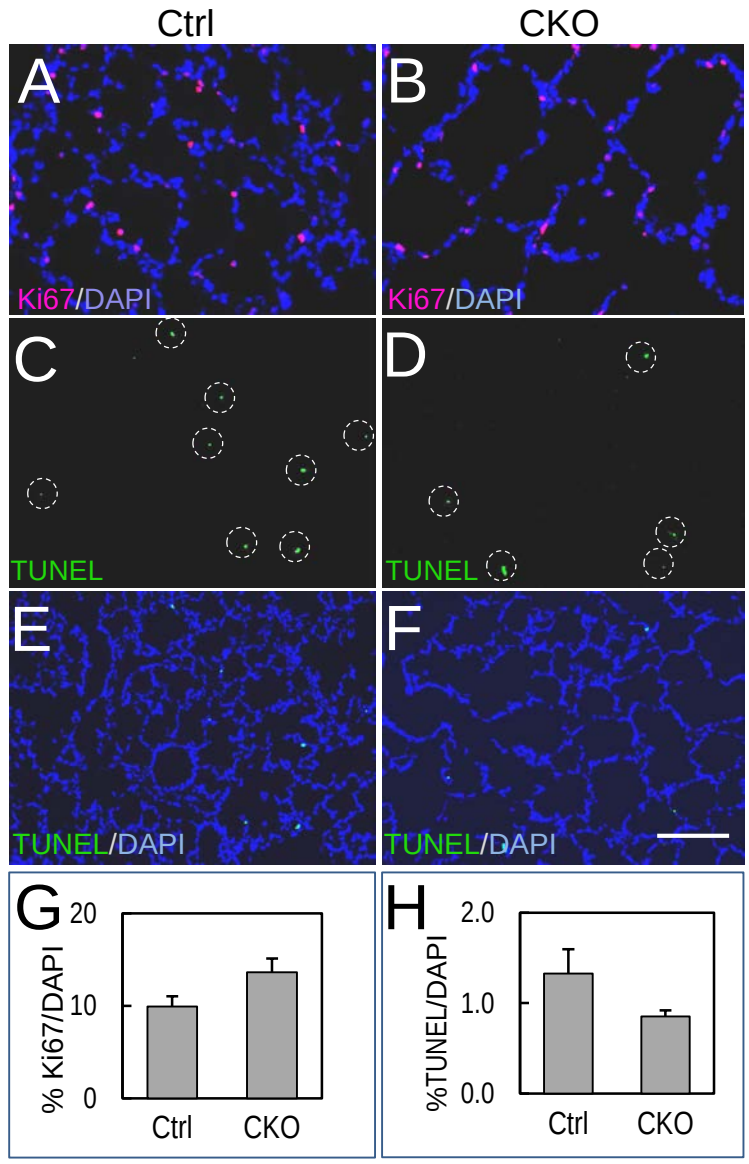

Figure S1. Comparison of proliferation and apoptosis between control and mutant lungs. (A&B) Immunostaining of Ki67 in PN14 control (A) and *Pdgfra*^{Gli1} lungs (CKO, B). **(C&D)** TUNEL staining in PN14 control (C) and *Pdgfra*^{Gli1} lungs (D). TUNEL positive cells were marked with white circles. **(E&F)** TUNEL staining of panels C & D with DAPI counter stain. **(G)** Ratio of Ki67^{pos} cells in total DAPI cells of PN14 lungs. **(H)** Ratio of TUNEL^{pos} cells in total DAPI cells of PN14 lungs. Multiple images from 3 Ctrl and 3 CKO lungs were analyzed (Ki67: n=8; TUNEL: n=8). Scale bar: 50 um for A&B, 100 um for C-F.

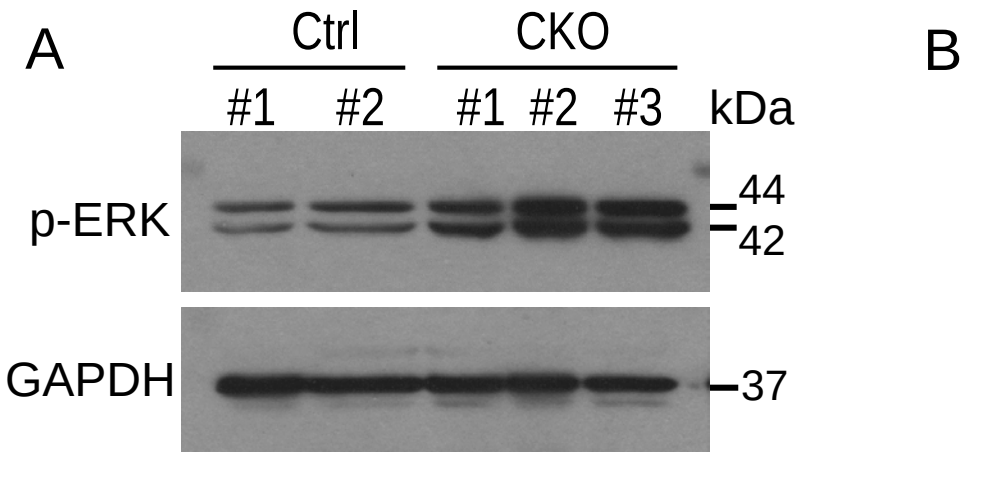

Figure S2. p-ERK is increased in *Pdgfra*^{Gli1} lungs. (A) Western blot of p-ERK in *Pdgfra*^{Gli1} (CKO) and control (Ctrl) lungs. Equal quantity of total protein extracts from 3 CKO and 2 littermate Ctrl lungs were loaded and GAPDH was used as loading control. **(B)** Quantification of western blot results shown in Panel A. Densitometric analysis of each band by NIH image J software, normalized to GAPDH. Ctrl values were arbitrarily set as unity.

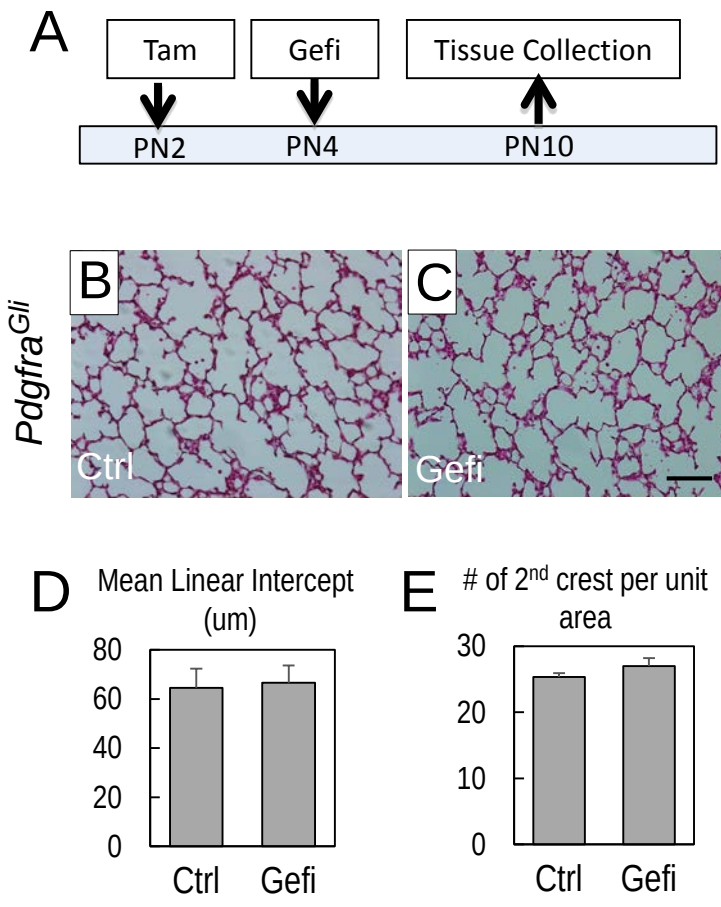

Figure S3. Gefitinib does not rescue the alveolar defect in *Pdgfra*^{Gli1} lungs. (A) Experimental design. **(B&C)** Hematoxylin and eosin (H&E) staining of *Pdgfra*^{Gli1} lungs from PN10 pups treated with carrier (Ctrl, B) or Gefitinib (Gefi, 50 ug/pup orally on PN4, C). Scale bar: 100 μm. Multiple H&E images (Ctrl: n=12; Gefi: n=18) from 2 Ctrl and 4 Gefi lungs were analyzed to obtain average mean linear intercept (MLI, **D**) and number of secondary crests per unit area **(E)**.

Table S1: Sequences of qRT-PCR primers

Gene name (mouse)	qPCR Primer Sequences
Pdgfra	5’-GTCGTTGACCTGCAGTGGA-3' 5’-CCAGCATGGTGATACCTTTGT-3'
Cd31	5’-GAGTACGAGGTGAAGGTGCAT-3' 5’-CGCCTTCTGTCACCTCCTT-3'
Vegfa	5’-CAGGCTGCTGTAACGATGAA-3' 5’-GCTTTGGTGAGGTTTGATCC-3'
Flk1	5’-CAGTGGTACTGGCAGCTAGAA-3' 5’-ACAAGCATACGGGCTTGTTT-3'
Adrp	5’-CCTCAGCTCTCCTGTTAGGC-3' 5’-CACTACTGCTGCTGCCATTT-3'
Ng2	5’-CTTGGCCTTGTTGGTCAGAT-3' 5’-CACCTCCAGGTGGTTCTCC-3'
Tgfb1	5'- TGG AGC AAC ATG TGG AAC TC -3' 5'- GTC AGC AGC CGG TTA CCA -3'
Tgfb2	5’-GAGAAAAATGCTTCGAATCTGG-3' 5’-TGGGAGATGTTAAGTCTTTGGAT-3'
Tgfb3	5’-CCCTGGACACCACTTCATGC-3' 5’-TCAATATAAAGGGGGCGTACA-3'
Igf1	5’-AGCAGCCTTCCAACTCAATTAT-3' 5’-TGAAGACGACATGATGTGTATCT-3'
Fgf2	5’-GACCCACACGTCAAACTACA-3' 5’-GCCGTCCATCTTCCTTCATAG-3'
Egf	5’-CGAATGGTGCAGTAGTAGATGC-3' 5’-GTCTCCATGAAGTCAGATGCAC-3'
Hbegf	5’-CCCCTATACACATATGACCACACT-3’ 5’-TCATAACCTCCTCTCCTGTGG-3’
Tgfa	5’-TGCTGCCACTCTGAGACAGT-3' 5’-TTGGTTGGGCTGTCATAGG-3'
Btc	5’-TGGTCATGGTGGTGTTCATC-3’ 5’-TTACGATGTTTCCGAAGAGGA-3’

Gene name (mouse)	qPCR Primer Sequences
Eln	5’-GCTGCTGCTAAGGCTGCTAA-3' 5’-AGCACCTGGGAGCCTAACTC-3'
Acta2 (aSma)	5’- CCCACCCAGAGTGGAGAA-3' 5’- ACATAGCTGGAGCAGCGTCT-3'
Loxl1	5’-TATGCCTGCACCTCTCACAC-3' 5’-TGTCCGCATTGTATGTGTCAT-3'
Loxl4	5’-AAGGAGTCCCATGCAGAGC-3' 5’-GGTTCATGAGCACTTCCACA-3’
Fbn2	5’-AAGAGGGTTCTCTCTGGATGC-3' 5’-CCCATCACACTCATCGACAT-3'
Fbln1	5’-GTGCAAGGCTGGCTTCTATT-3' 5’-GATAGCGCTGGCACTCGT-3'
Fbln2	5’-TGTTGTTGGGGACACAGCTA-3' 5’-CCATCAAACACTCGTCTTGGT-3'
Fbln5	5’-TTGAGGAAGATGGCATTCACT-3' 5’-GGCTGGTTCACACACTCGT-3'
Aqp5	5’-CAGACCTCAGAGATTGTGAAG-3' 5’- CAGAAATAAATAAGATGGCAC-3'
Hopx	5’-ACCACGCTGTGCCTCATC-3' 5’-GCGCTGCTTAAACCATTTCT-3'
Pdpn(T1a)	5’-CAGTGTTGTTCTGGGTTTTGG-3' 5’-TGGGGTCACAATATCATCTTCA-3'
Rage	5’-GTGTCGGGCAACTAACAGG-3' 5’-CTGGCTTCCCAGGAATCTG-3'
Sftpa (SpA)	5’-CTGGAGAACATGGAGACAAGG-3' 5’-AAGCTCCTCATCCAGGTAAGC-3'
Sftpb (SpB)	5’-AACCCCACACCTCTGAGAAC-3' 5’-GTGCAGGCTGAGGCTTGT-3'
Sftpc (Spc)	5’-GGTCCTGATGGAGAGTCCAC-3' 5’-GATGAGAAGGCGTTTGAGGT-3'

Gene name (human)	qPCR Primer Sequences
LOXL1	5’-GCATGCACCTCTCATACCC-3' 5’-CAGTCGATGTCCGCATTGTA-3'
LOXL4	5’-CCAGCTTCTGTCTGGAGGAC-3' 5’-AAGTTGGCACATGCGTAGC-3'
FBN2	5’-GCTGCGAGTGTGAGATGG-3' 5’-TTTGGAAGGAGCATTCATCA-3'
FBLN5	5’-CTGCCCTCCAGGCTACATC-3' 5’-CCTGTGCTCACATTCGTTGA-3'
ELN	5’-GGAGGTGTTCCCGGAGTC-3' 5’-GGTCCCCACTCCGTACTTG-3'
PDGFRa	5’-CCACCTGAGTGAGATTGTGG-3' 5’-TCTTCAGGAAGTCCAGGTGAA-3'
TGFA	5’-GCTTGCTGCCACTCAGAAA-3' 5’-TTATTGATCTGCCACAGTCCA-3'
BTC	5’-ACTGCATCAAAGGGAGATGC-3' 5’-TCTCACACCTTGCTCCAATG-3'
EGF	5’-ACACATGCTAGTGGCTGAAA-3' 5’-GCATCCTCTCCCTCTGAAATAC-3'
HB-EGF	5’-TGGGGCTTCTCATGTTTAGG-3' 5’-CATGCCCAACTTCACTTTCTC-3'
IGF1	5’-TGTGGAGACAGGGGCTTTTA-3' 5’-ATCCACGATGCCTGTCTGA-3'

Table S2: Antibody information

Anitbody & Reagents	**Company**	**Catelog #**
mouse anti-GFP (1:100)	Santa Cruz, CA	SC-9996
rabbit anti-ACTA2 (1:300)	Abcam, MA	AB5694
rabbit anti-PDGFRa (1:50)	Cell Signaling, MA	3174
rabbit anti-proSPC (1:200)	EMD Millipore Corp. MA	AB3786
rabbit anti-HOPX (1:50)	Santa Cruz, CA	SC-30216
rabbit anti-tropoelastin (1:200)	Abcam, MA	AB21600
rabbit anti-Ki67 (1:50)	Thermo Fisher Scientific, CA	RM-9106-s1
sheep anti-Ki67 (1:50)	R&D systems, MN	AF7649
goat anti-EMCN (1:100)	R&D systems, MN	AF4666
Imatinib	Cayman Chemical, MI	13139
Gefitinib	Cayman Chemical, MI	13166
EGF	R&D Systems, MN	236-EG
TGFb1	Leinco Technologies, MO	T170

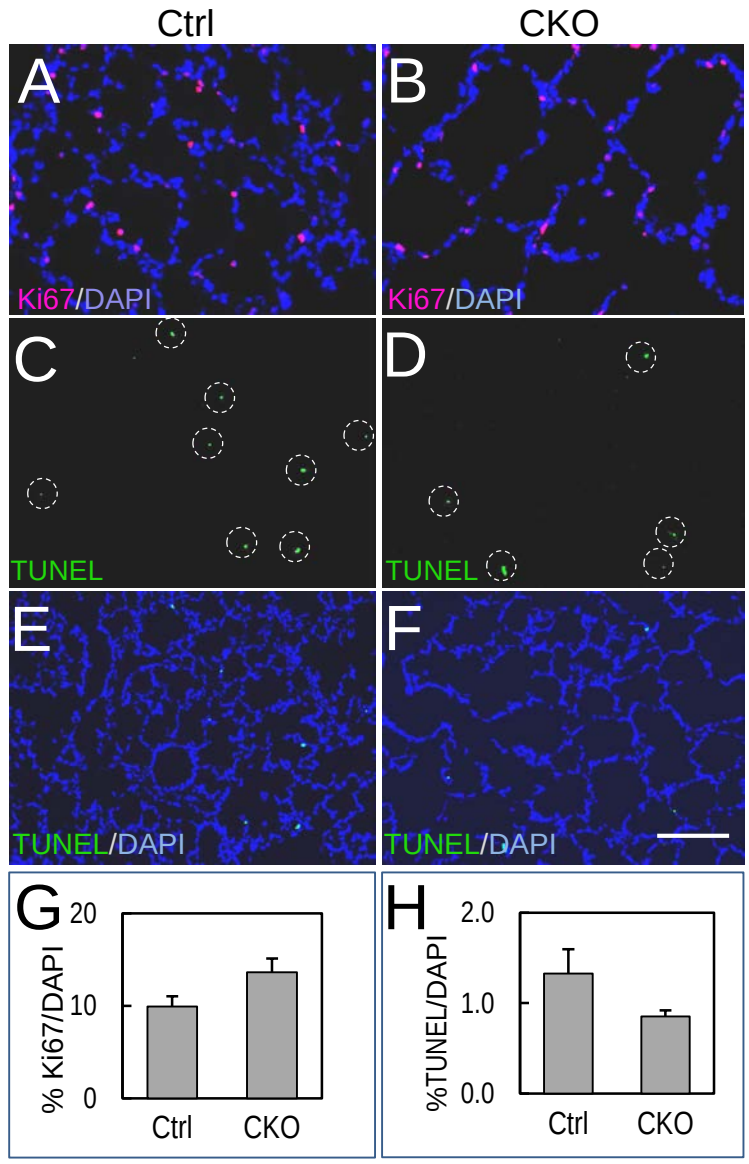

Figure S1. Comparison of proliferation and apoptosis between control and mutant lungs. (A&B) Immunostaining of Ki67 in PN14 control (A) and *Pdgfra*^{Gli1} lungs (CKO, B). **(C&D)** TUNEL staining in PN14 control (C) and *Pdgfra*^{Gli1} lungs (D). TUNEL positive cells were marked with white circles. **(E&F)** TUNEL staining of panels C & D with DAPI counter stain. **(G)** Ratio of Ki67^{pos} cells in total DAPI cells of PN14 lungs. **(H)** Ratio of TUNEL^{pos} cells in total DAPI cells of PN14 lungs. Multiple images from 3 Ctrl and 3 CKO lungs were analyzed (Ki67: n=8; TUNEL: n=8). Scale bar: 50 um for A&B, 100 um for C-F.

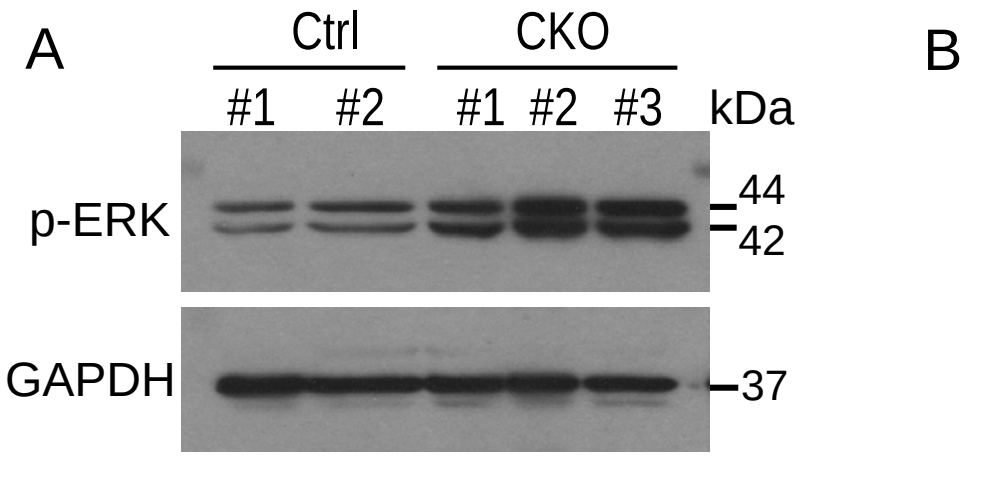

Figure S2. p-ERK is increased in *Pdgfra*^{Gli1} lungs. (A) Western blot of p-ERK in *Pdgfra*^{Gli1} (CKO) and control (Ctrl) lungs. Equal quantity of total protein extracts from 3 CKO and 2 littermate Ctrl lungs were loaded and GAPDH was used as loading control. **(B)** Quantification of western blot results shown in Panel A. Densitometric analysis of each band by NIH image J software, normalized to GAPDH. Ctrl values were arbitrarily set as unity.

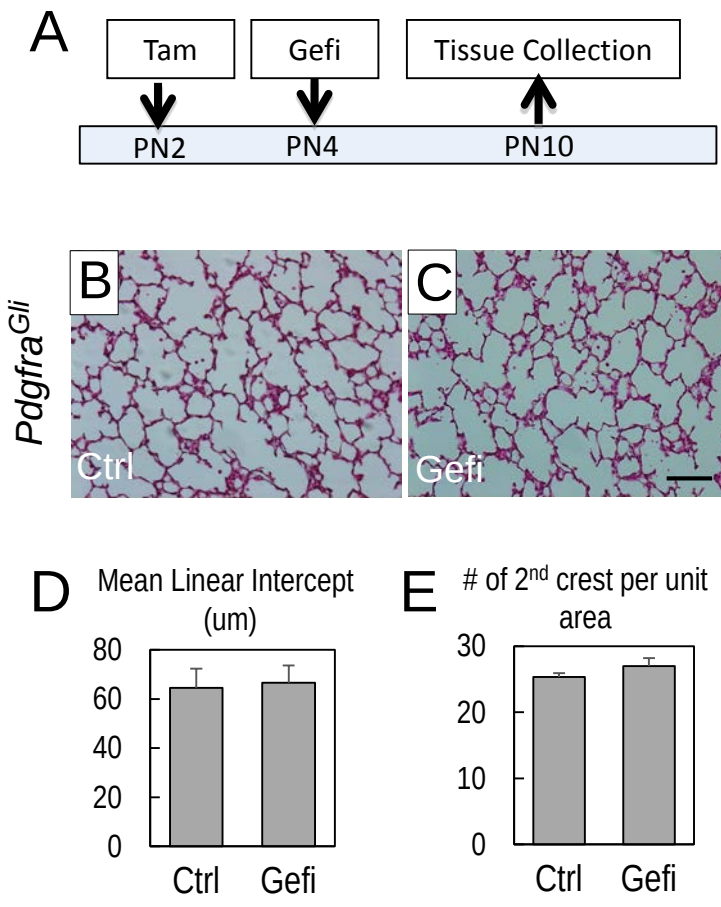

Figure S3. Gefitinib does not rescue the alveolar defect in *Pdgfra*^{Gli1} lungs. (A) Experimental design. **(B&C)** Hematoxylin and eosin (H&E) staining of *Pdgfra*^{Gli1} lungs from PN10 pups treated with carrier (Ctrl, B) or Gefitinib (Gefi, 50 ug/pup orally on PN4, C). Scale bar: 100 μm. Multiple H&E images (Ctrl: n=12; Gefi: n=18) from 2 Ctrl and 4 Gefi lungs were analyzed to obtain average mean linear intercept (MLI, **D**) and number of secondary crests per unit area **(E)**.

Table S1: Sequences of qRT-PCR primers

Gene name (mouse)	qPCR Primer Sequences
Pdgfra	5’-GTCGTTGACCTGCAGTGGA-3' 5’-CCAGCATGGTGATACCTTTGT-3'
Cd31	5’-GAGTACGAGGTGAAGGTGCAT-3' 5’-CGCCTTCTGTCACCTCCTT-3'
Vegfa	5’-CAGGCTGCTGTAACGATGAA-3' 5’-GCTTTGGTGAGGTTTGATCC-3'
Flk1	5’-CAGTGGTACTGGCAGCTAGAA-3' 5’-ACAAGCATACGGGCTTGTTT-3'
Adrp	5’-CCTCAGCTCTCCTGTTAGGC-3' 5’-CACTACTGCTGCTGCCATTT-3'
Ng2	5’-CTTGGCCTTGTTGGTCAGAT-3' 5’-CACCTCCAGGTGGTTCTCC-3'
Tgfb1	5'- TGG AGC AAC ATG TGG AAC TC -3' 5'- GTC AGC AGC CGG TTA CCA -3'
Tgfb2	5’-GAGAAAAATGCTTCGAATCTGG-3' 5’-TGGGAGATGTTAAGTCTTTGGAT-3'
Tgfb3	5’-CCCTGGACACCACTTCATGC-3' 5’-TCAATATAAAGGGGGCGTACA-3'
Igf1	5’-AGCAGCCTTCCAACTCAATTAT-3' 5’-TGAAGACGACATGATGTGTATCT-3'
Fgf2	5’-GACCCACACGTCAAACTACA-3' 5’-GCCGTCCATCTTCCTTCATAG-3'
Egf	5’-CGAATGGTGCAGTAGTAGATGC-3' 5’-GTCTCCATGAAGTCAGATGCAC-3'
Hbegf	5’-CCCCTATACACATATGACCACACT-3’ 5’-TCATAACCTCCTCTCCTGTGG-3’
Tgfa	5’-TGCTGCCACTCTGAGACAGT-3' 5’-TTGGTTGGGCTGTCATAGG-3'
Btc	5’-TGGTCATGGTGGTGTTCATC-3’ 5’-TTACGATGTTTCCGAAGAGGA-3’

Gene name (mouse)	qPCR Primer Sequences
Eln	5’-GCTGCTGCTAAGGCTGCTAA-3' 5’-AGCACCTGGGAGCCTAACTC-3'
Acta2 (aSma)	5’- CCCACCCAGAGTGGAGAA-3' 5’- ACATAGCTGGAGCAGCGTCT-3'
Loxl1	5’-TATGCCTGCACCTCTCACAC-3' 5’-TGTCCGCATTGTATGTGTCAT-3'
Loxl4	5’-AAGGAGTCCCATGCAGAGC-3' 5’-GGTTCATGAGCACTTCCACA-3’
Fbn2	5’-AAGAGGGTTCTCTCTGGATGC-3' 5’-CCCATCACACTCATCGACAT-3'
Fbln1	5’-GTGCAAGGCTGGCTTCTATT-3' 5’-GATAGCGCTGGCACTCGT-3'
Fbln2	5’-TGTTGTTGGGGACACAGCTA-3' 5’-CCATCAAACACTCGTCTTGGT-3'
Fbln5	5’-TTGAGGAAGATGGCATTCACT-3' 5’-GGCTGGTTCACACACTCGT-3'
Aqp5	5’-CAGACCTCAGAGATTGTGAAG-3' 5’- CAGAAATAAATAAGATGGCAC-3'
Hopx	5’-ACCACGCTGTGCCTCATC-3' 5’-GCGCTGCTTAAACCATTTCT-3'
Pdpn(T1a)	5’-CAGTGTTGTTCTGGGTTTTGG-3' 5’-TGGGGTCACAATATCATCTTCA-3'
Rage	5’-GTGTCGGGCAACTAACAGG-3' 5’-CTGGCTTCCCAGGAATCTG-3'
Sftpa (SpA)	5’-CTGGAGAACATGGAGACAAGG-3' 5’-AAGCTCCTCATCCAGGTAAGC-3'
Sftpb (SpB)	5’-AACCCCACACCTCTGAGAAC-3' 5’-GTGCAGGCTGAGGCTTGT-3'
Sftpc (Spc)	5’-GGTCCTGATGGAGAGTCCAC-3' 5’-GATGAGAAGGCGTTTGAGGT-3'

Gene name (human)	qPCR Primer Sequences
LOXL1	5’-GCATGCACCTCTCATACCC-3' 5’-CAGTCGATGTCCGCATTGTA-3'
LOXL4	5’-CCAGCTTCTGTCTGGAGGAC-3' 5’-AAGTTGGCACATGCGTAGC-3'
FBN2	5’-GCTGCGAGTGTGAGATGG-3' 5’-TTTGGAAGGAGCATTCATCA-3'
FBLN5	5’-CTGCCCTCCAGGCTACATC-3' 5’-CCTGTGCTCACATTCGTTGA-3'
ELN	5’-GGAGGTGTTCCCGGAGTC-3' 5’-GGTCCCCACTCCGTACTTG-3'
PDGFRa	5’-CCACCTGAGTGAGATTGTGG-3' 5’-TCTTCAGGAAGTCCAGGTGAA-3'
TGFA	5’-GCTTGCTGCCACTCAGAAA-3' 5’-TTATTGATCTGCCACAGTCCA-3'
BTC	5’-ACTGCATCAAAGGGAGATGC-3' 5’-TCTCACACCTTGCTCCAATG-3'
EGF	5’-ACACATGCTAGTGGCTGAAA-3' 5’-GCATCCTCTCCCTCTGAAATAC-3'
HB-EGF	5’-TGGGGCTTCTCATGTTTAGG-3' 5’-CATGCCCAACTTCACTTTCTC-3'
IGF1	5’-TGTGGAGACAGGGGCTTTTA-3' 5’-ATCCACGATGCCTGTCTGA-3'

Table S2: Antibody information

Anitbody & Reagents	**Company**	**Catelog #**
mouse anti-GFP (1:100)	Santa Cruz, CA	SC-9996
rabbit anti-ACTA2 (1:300)	Abcam, MA	AB5694
rabbit anti-PDGFRa (1:50)	Cell Signaling, MA	3174
rabbit anti-proSPC (1:200)	EMD Millipore Corp. MA	AB3786
rabbit anti-HOPX (1:50)	Santa Cruz, CA	SC-30216
rabbit anti-tropoelastin (1:200)	Abcam, MA	AB21600
rabbit anti-Ki67 (1:50)	Thermo Fisher Scientific, CA	RM-9106-s1
sheep anti-Ki67 (1:50)	R&D systems, MN	AF7649
goat anti-EMCN (1:100)	R&D systems, MN	AF4666
Imatinib	Cayman Chemical, MI	13139
Gefitinib	Cayman Chemical, MI	13166
EGF	R&D Systems, MN	236-EG
TGFb1	Leinco Technologies, MO	T170